THE JOURNAL OF BIOLOGICAL CHEMISTRY VOL. 289, NO. 14, pp. 9936–9951, April 4, 2014
Published in the U.S.A.

Mitochondrial Targeting of Cytochrome P450 (CYP) 1B1 and Its Role in Polycyclic Aromatic Hydrocarbon-induced Mitochondrial Dysfunction*

Received for publication, October 9, 2013, and in revised form, January 15, 2014 Published, JBC Papers in Press, February 4, 2014, DOI 10.1074/jbc.M113.525659

Seema Bansal[‡], Adrian N. Leu[‡], Frank J. Gonzalez[§], F. Peter Guengerich[¶], Anindya Roy Chowdhury[‡], Hindupur K. Anandatheerthavarada[‡], and Narayan G. Avadhani[‡1]

From the [‡]Department of Animal Biology and the Mari Lowe Center for Comparative Oncology, School of Veterinary Medicine, University of Pennsylvania, Philadelphia, Pennsylvania 19104, the [§]Laboratory of Metabolism, Center for Cancer Research, NCI, National Institutes of Health, Bethesda, Maryland 20892, and the [¶]Department of Biochemistry and Center in Molecular Toxicology, Vanderbilt University School of Medicine, Nashville, Tennessee 37232

Background: Cytochrome P450 (CYP) 1B1 activates diverse polycyclic aromatic hydrocarbons (PAH) to reactive species.
Results: Processing by a cytosolic Ser protease activates a mitochondrial (mt) targeting signal of CYP1B1.
Conclusion: Mitochondrial CYP1B1 plays a role in PAH-induced mtDNA damage and mitochondrial dysfunction.
Significance: PAH-induced mitochondrial dysfunction may be important in tissue injury and inflammation.

We report that polycyclic aromatic hydrocarbon (PAH)-inducible CYP1B1 is targeted to mitochondria by sequence-specific cleavage at the N terminus by a cytosolic Ser protease (polyserase 1) to activate the cryptic internal signal. Site-directed mutagenesis, COS-7 cell transfection, and *in vitro* import studies in isolated mitochondria showed that a positively charged domain at residues 41–48 of human CYP1B1 is part of the mitochondrial (mt) import signal. Ala scanning mutations showed that the Ser protease cleavage site resides between residues 37 and 41 of human CYP1B1. Benzo[*a*]pyrene (BaP) treatment induced oxidative stress, mitochondrial respiratory defects, and mtDNA damage that was attenuated by a CYP1B1-specific inhibitor, 2,3,4,5-tetramethoxystilbene. In support, the mitochondrial CYP1B1 supported by mitochondrial ferredoxin (adrenodoxin) and ferredoxin reductase showed high aryl hydrocarbon hydroxylase activity. Administration of benzo[*a*]pyrene or 2,3,7,8-tetrachlorodibenzodioxin induced similar mitochondrial functional abnormalities and oxidative stress in the lungs of wild-type mice and *Cyp1a1/1a2*-null mice, but the effects were markedly blunted in *Cyp1b1*-null mice. These results confirm a role for CYP1B1 in inducing PAH-mediated mitochondrial dysfunction. The role of mitochondrial CYP1B1 was assessed using A549 lung epithelial cells stably expressing shRNA against NADPH-cytochrome P450 oxidoreductase or mitochondrial adrenodoxin. Our results not only show conservation of the endoprotease cleavage mechanism for mitochondrial import of family 1 CYPs but also reveal a direct role for mitochondrial CYP1B1 in PAH-mediated oxidative and chemical damage to mitochondria.

Polycyclic aromatic hydrocarbons (PAHs)[2] induce an array of genes involved in a wide range of tissue pathologies, including inflammation, immune response, drug toxicity, and cancer that are predominantly elicited through activation of the aryl hydrocarbon receptor (Ahr). The Ahr-regulated CYP1 family genes, particularly CYP1A1 and CYP1B1, play a central role in the metabolic activation and clearance of a diverse class of PAHs and heterocyclic amines/amides, which cause carcinogenesis in multiple tissues (1–9). The other member of this family, CYP1A2, appears to have very low activity for several PAHs but actively metabolizes aflatoxin B1, acetaminophen, and food-derived aromatic amines (10). All three members of the CYP1 genes are transcriptionally activated by Ahr binding to the xenobiotic-response element as a heterodimer with aryl hydrocarbon nuclear translocator on the promoter-enhancer sites (9, 11, 12). Ahr is activated by PAHs, heterocyclic amines/amides, and polychlorinated biphenyls present in the environmental pollution and cigarette smoke. Of the three CYP family 1 enzymes induced by Ahr, CYP1B1 is recognized as an extrahepatic enzyme expressed in steroidogenic tissues and the vascular compartments of lung, heart, prostate, and parts of the brain (13–18). CYP1B1 is also overexpressed in lymphomas and tumors of the breast, endometrium, ovarian, prostate, and lung (19, 20), and therefore it has emerged as having a potential role in many tumors.

The human *CYP1B1* gene has been implicated in playing a prominent role in multi-tissue carcinogenesis, and CYP1B1 knock-out mice (*Cyp1b1*-null) displayed a markedly reduced

* This work was supported, in whole or in part, by National Institutes of Health Grants R01 GM34883 (to N. G. A.) and Grant R37 CA090426 (to F. P. G.). This work was also supported by the Harret Ellison Woodward Trust (to N. G. A).

[1] To whom correspondence should be addressed: Dept. of Animal Biology and the Mari Lowe Center for Comparative Oncology, School of Veterinary Medicine, University of Pennsylvania, Philadelphia, PA 19104. Tel.: 215-898-8819; Fax: 215-573-6810; E-mail: Narayan@vet.upenn.edu.

[2] The abbreviations used are: PAH, polycyclic aromatic hydrocarbon; CYP, cytochrome P450; NPR, NADPH-cytochrome P450 reductase; Adx, adrenodoxin; AdxR, adrenodoxin reductase; ER, endoplasmic reticulum; BaP, benzo[*a*]pyrene; TCDD, 2,3,7,8-tetrachlorodibenzodioxin; AHH, aryl hydrocarbon hydroxylase; Ahr, aryl hydrocarbon receptor; CcO, cytochrome *c* oxidase; SDH, succinate dehydrogenase; TMS, 2,3,4,5-tetramethoxystilbene; SOD, superoxide dismutase; ROS, reactive oxygen species; DHFR, dihydrofolate reductase; Tricine, *N*-[2-hydroxy-1,1-bis(hydroxymethyl)ethyl]glycine; NPR, NADPH cytochrome P450 reductase; DCFH-DA, dichlorodihydrofluorescein diacetate.

incidence of 7,12-dimethlybenz[*a*]anthracene-induced lymphomas (21). CYP1B1 is also considered as a biomarker for hormone-mediated cancers (*e.g.* breast, endometrium, ovarian, and prostate), and the etiology of these cancers is mostly related to the level of the sex hormones estrogen and testosterone (1, 19, 22, 23). Some epidemiological studies also suggest correlation between the L432N polymorphism of CYP1B1 and breast cancer. In support, CYP1B1 was shown to oxidize 17-β-estradiol into 4- and 2-hydroxy products with widely different affinities for binding to the estrogen receptor (22, 24–28). In addition to the proposed role in carcinogenesis, CYP1B1 is also involved in primary congenital glaucoma (29). Studies by Bagiveva *et al.*, (30) also suggested impaired localization and impaired enzyme activity of CYP1B1 as possible factors in primary congenital glaucoma.

Studies from our laboratories and others have conclusively established that several of the ER-targeted CYPs are also bimodally targeted to mitochondria because of a stretch of N-terminal chimeric signals (31–39). We hypothesized that the 10–15 amino acids immediately past the ER targeting and membrane anchor region, rich in positively charged residues in various inducible and constitutively expressed CYPs, function as cryptic mitochondria targeting signals that are activated by physiological factors. We described two distinct mechanisms for the activation of cryptic signals as follows:

1) PKA- and/or PKC-mediated phosphorylation at the N-terminal phosphorylation sites of CYP2B1, CYP2E1, and CYP2D6 and C-terminal sites of glutathione transferases, increasing the affinity of nascent chains for binding to the mitochondrial chaperones HSP70 and HSP90 (33, 39–43);
2) sequence-specific endoprotease processing past the N-terminal transmembrane domain by a xenobiotic-inducible Ser protease in the case of CYP1A1, as a mechanism of activation of cryptic signal (32, 35, 37, 44). This mechanism is conserved in the murine and possibly in other systems based on the position of the conserved serine protease processing site immediately past the transmembrane domain (35). Our studies also showed that CYPs that are imported into mitochondria exist as membrane extrinsic proteins and functionally interact with mitochondrial soluble electron transport proteins in the metabolism of different substrates (45).

In this study, we show that CYP1B1 contains a chimeric signal similar to that of CYP1A1 and is also bimodally targeted to mitochondria. We show that nascent CYP1B1 protein is processed in the cytosol between amino acid residues 38 and 41 (of the nascent protein) for activating the cryptic signal, suggesting the conservation of signal activation and targeting mechanism for the CYP1 family proteins. Furthermore, using knock-out animal models, we show that CYP1B1 plays a major role in BaP and TCDD-mediated mitochondrial respiratory defects, overproduction of reactive oxygen species (ROS) mitochondrial DNA (mtDNA), and membrane damage in the pulmonary tissue. Use of A549 lung epithelial cells expressing shRNA against NPR and Adx show that mitochondrial CYP1B1 is likely to be responsible for the BaP- and TCDD-induced mitochondrial dysfunction.

EXPERIMENTAL PROCEDURES

Sources of Antibodies—Polyclonal antibodies to human CYP1B1 (in rabbit), porin (in rabbit), and SDH (in mouse) were purchased from Abcam (Cambridge, MA). Antibodies to human cytochrome *c* oxidase subunit 1 (CcOI) (anti-mouse), human subunit Vb (CcOVb) (anti-mouse), and human cytochrome oxidase IVi1 (CcO IVi1) (anti-rabbit) were from Mitosciences (Eugene, OR). Antibodies raised against human NPR (anti-mouse) and TOM20 (anti-rabbit) were from Santa Cruz Biotechnology, Santa Cruz, CA.

Treatment of Animals and Tissue Fractionation—All animal procedures were carried out in compliance with the National Institutes of Health guidelines for the use of vertebrate animals and were approved by the University of Pennsylvania's IACUC for the use of animals. Male C57BL/6N WT mice and CYP1B1 knock-out (*Cyp1b1*-null) mice (20–25 g) received BaP (12.5 mg/kg body weight) daily for 14 days by oral gavage and TCDD (30 μg/kg body weight) daily for 3 days. The rationale for oral administration of BaP was based on the observation by Nebert and co-workers (46) that inhaled pollutants not only enter the lung but that the majority of particles are swallowed; hence, there exists a need to understand the toxicological parameters of orally administered PAHs. The control mice received equivalent volumes of corn oil. The animals were killed by CO_2 asphyxiation 24 h after the last gavage/injection and perfused transcardially with ice-cold saline. The lungs were then rapidly removed and rinsed with saline, and the lung microsomes and mitochondria were isolated as described previously (47) using H-medium. The mitochondrial and microsomal isolates were suspended in 50 mM potassium phosphate buffer, pH 7.5, containing 20% (v/v) glycerol, 0.1 mM EDTA, 0.1 mM DTT, and 0.1 mM PMSF and used for various assays.

Growth and Treatment of Cells—Human breast carcinoma MCF-7 cells (ATCC HTB-22^{TM}) were grown in Dulbecco's Eagle's minimum essential medium (DMEM) with 0.01 mg/ml bovine insulin, 10% fetal bovine serum (v/v), 100 units/ml penicillin, and 100 μg/ml streptomycin. Human lung carcinoma A549 cells (ATCC CCL-185) and African Green Monkey Kidney COS-7 cells (ATCC CRL-1651) were grown in DMEM with 10% fetal bovine serum (v/v) with 1% (w/v) penicillin/streptomycin added. Cells were maintained at 37 °C in a humidified atmosphere made of 5% CO_2 and 95% air (v/v). DMSO, when added, was at a final concentration of 0.1% (v/v), which does not affect cellular functions and integrity. BaP, at a concentration of 20 μM, was used for the induction of CYP1B1. 2,3,4,5-Tetramethoxystilbene (TMS), a CYP1B1-selective inhibitor, was used at a concentration of 10 μg/ml. Proadifen hydrochloride (SKF525A), a general inhibitor of CYPs, was used at a concentration of 1 mM. Control plates were treated with an equivalent volume of 0.1% DMSO (v/v) alone.

Hazardous Chemicals—While handling BaP and TCDD, personnel were required to observe safe handling procedures, and almost all procedures dealing with these chemicals were carried out in a hood. Personnel were required to wear lab coats, gloves, bonnets, and masks at all times, and contaminated materials were collected and stored safely for disposal by the Hazardous Waste Unit (EHRS) of the University.

Construction of Plasmids—Full-length CYP1B1 (WT) was amplified from cDNA isolated from TCDD-treated A549 human lung carcinoma cells in fragments and joined by overlap PCR. The N-terminal truncations (+34, +54, and +141) were generated by PCR amplification using appropriate primers containing cloning sites. All constructs were cloned in HindIII and XbaI sites in PCDNA3.1 for *in vitro* import and into a PCMV4 vector for cell transfection studies. All constructs were also engineered to contain an ATG codon preceded by a Kozak consensus sequence. The mouse dihydrofolate reductase (DHFR) cDNA was fused in-frame through a BamHI linker to the N terminus of WT CYP1B1, referred to hereafter as DHFR-1B1, and was cloned into a PCMV4 vector. The mitochondrial targeting mutants Rmut1 and Rmut2 were generated using a QuikChange site-directed mutagenesis kit (Agilent Technologies, Santa Clara, CA). In Rmut1, Arg residues at position 41 and positions 43–45 were mutated to Ala. In Rmut2, Arg residues at positions 43–45 and 48 were mutated to Ala for identifying the mitochondrial targeting signal. Ala substitutions at the 37/38(M1), 38/39(M2), 39/40(M3), and 40/41(M4) sites were also carried out in CYP1B1 WT and DHFR-CYP1B1 for characterizing the putative protease-processing sites. The primers used are listed in Table 1.

Transient Transfection of WT and Mutant CYP1B1 in COS-7 Cells—COS-7 cells were the preferred system for transient expression because of a lack of endogenous CYP gene expression and also because of high transfection efficiency with these cells. Cells were transiently transfected with cDNA constructs using FuGENE HD transfection reagent (Roche Diagnostics). The transfection reagent/DNA ratio was maintained at 3:2. After 48 h of transfection, cells were harvested, washed in 1× phosphate-buffered saline (PBS: 137 mM NaCl, 2.7 mM KCl, 8.1 mM Na_2HPO_4, 1.5 mM KH_2PO_4, pH 7.4), and used for subcellular fractionation as described above.

Isolation of Mitochondria, Microsomes, and Total Extract from COS-7 Cells—Cells were washed twice with ice-cold PBS and lysed in lysis buffer (25 mM Tris-HCl, pH 7.4, 150 mM NaCl, 0.1 mM EDTA, 1% Nonidet P-40 (v/v), 0.1% deoxycholate (w/v), 0.025% NaN_3 (w/v), 1% protease inhibitor mixture from Roche Diagnostics) to prepare cellular extract. Mitochondria and microsomes were isolated by differential centrifugation (37) using a sucrose/mannitol buffer system (20 mM potassium HEPES, pH 7.5, containing 70 mM sucrose, 220 mM mannitol, and 2 mM EDTA). The mitochondrial pellet was resuspended in sucrose/mannitol buffer and sedimented through 1.0 M sucrose at 8500 × *g* for 20 min to minimize contaminating membranes. The post-mitochondrial supernatant was centrifuged at 100,000 × *g* for 90 min to pellet microsomes. Mitochondria and microsomes were resuspended in 50 mM potassium phosphate buffer, pH 7.5, containing 20% glycerol (v/v), 0.1 mM EDTA, 0.1 mM dithiothreitol, and 0.1 mM phenylmethanesulfonyl fluoride. Mitochondria were treated with digitonin (75 μg/mg protein on ice for 3 min) as described previously (37). Freshly isolated mitochondria and microsomes were treated with trypsin (100 μg/mg in 0.2 ml of reaction volume for 30 min at 4 °C), followed by treatment with trypsin inhibitor (300 μg/mg mitochondrial protein) as described previously (48). The mitochondrial and microsomal proteins (50 μg each), solubilized in 2× Laemmli sample buffer (49), were resolved by electrophoresis on 12–14% SDS-polyacrylamide gels.

TABLE 1
Primers used for constructing plasmids and introducing mutations

Overlap PCR primers to generate WT and N-terminal truncation mutants
FP1, TCA AGC TTA CCA TGG GCA CCA GCC TCA GC
RP1, GAA CTT GTC CAG GAT GAA GTT GCT GAA G
FP2, CTT CAG CAA CTT CAT CCT GGA CAA GTT C
RP2, TCT CTA GAC TTA TTG GCA AGT TTC CTT GGC T
+34 1B1, AA GCT TGC CAC CAT GG TGC ATG TGG GCC AGC GG
+54 1B1, AAG CTT GCC ACC ATG GGC CCG TTT GCG TGG CCA CTG
+141 1B1, AAG CTT GCC ACC ATG GCA TGG AAG GTG CAG CGG
Mutants generation and DHFR-1B1 fusion construct
RMut1
FP, CGG CTG CTG GCG CAA GCG GCG GCG CAG CTC CGG TCC GCG
RP, CGC GGA CCG GAG CTG TGC TGC TGC TTG TGC CAG CAG CCG
RMut2
FP, CTG AGG CAA GCG GCG GCG CAG CTC GCC TCC GCG CCC CCG
RP, CGG GGG CGC GGA TGC GAG CTG TGC TGC TGC TTG CCT CAG
Mouse DHFR
FP, TCA AGC TTA CCA TGG TTC GAC CAT TGA ACT GC
RP, TCG GAT CCG TCT TTC TTC TCG TAG ACT TC
DHFR 1B1, TCG GAT CCG GCA CCA GCC TCA GCC CGA ACG AC
MUT37/38 (M1)
FP, 5′-GCCACTGTGCATGTGGGCGCGGCGCTGCTGAGGCAAC GGAGGCGGC
RP, 5′-GCCGCCTCCGTTGCCTCAGCAGCGCCGCGCCCACATG CACAGTGGC
MUT38,39 (M2)
FP, 5′-GCCACTGTGCATGTGGGCCAGGCGGCGCTGAGGCAAC GGAGGCGGC
RP, 5′-GCCGCCTCCGTTGCCTCAGCGCCGCCTGGCCCACATG CACAGTGGC
MUT39,40 (M3)
FP, 5′-GCCACTGTGCATGTGGGCCAGCGGGCGGCGAGGCAAC GGAGGCGGC
RP, 5′-GCCGCCTCCGTTGCCTCGCCGCCCGCTGGCCCACATG CACAGTGGC
MUT 40,41(M4)
FP, 5′-GCCACTGTGCATGTGGGCCAGCGGCTGGCGGCGCAAC GGAGGCGGC
RP, 5′-GCCGCCTCCGTTGCGCCGCCAGCCGCTG GCCCACATGCACAGTGGC
Generation of Adx and NPR shRNA
Adx shRNA, TGATGGTGAAACATTAACAACCAAAGGAA
NPR shRNA, CAGAACACCTTCTACGACATCGTGGCTGA

Analysis of Cellular Respiration (Seahorse XF24 System)—The oxygen consumption rates were measured using an XF24 high sensitivity respirometer (Seahorse Bioscience, Billerica, MA) as described previously (50), following the manufacturer's instructions. Briefly, 50,000 cells (with or without BaP treatment (20 μM) and with or without TMS (0.8 μg/ml)) were cultured in DMEM for 16 h, and the medium was replaced with XF assay medium (low buffered bicarbonate-free DMEM, pH 7.4) before measurements. The cells were incubated at 37 °C for 30 min to allow media temperature and pH to reach equilibrium before the first rate measurement. Oligomycin (2 μg/ml), 2,4-dinitrophenol (a mitochondrial uncoupler, 75 μM), or the complex I inhibitor rotenone (1 μM) were injected through the cartridge, and oxygen consumption rates were measured under basal conditions as well as after sequential injections of oligomycin, 2,4-dinitrophenol, and rotenone following the calibration procedure (30 min calibration, 10 min rest). Measurement cycles of 1-min sample mixing, 2 min waiting, and 3 min measurement of oxygen consumption rate were carried out. The

cell numbers and concentrations of inhibitors used were optimized. The difference in the cell density between wells was corrected on the basis of β-actin level determined by immunoblot analysis. Absolute rates of oxygen consumption were linearly related to cell numbers seeded within the measurement range. Measurements were carried out in triplicate wells.

Alkaline Extraction of Membrane Proteins—The membrane topology of mitochondrial CYP was determined by extraction with alkaline Na_2CO_3 using a procedure modified from Clark and Waterman (51). The insoluble pellet and the soluble protein fractions were solubilized in 10 mM Tris-HCl (pH 7.0, containing 2% SDS (w/v)) and used for immunoblot analysis (38).

Aryl Hydrocarbon Hydroxylation (AHH) Activity—AHH activity (using BaP as a substrate) was assayed using a spectrofluorometric method, following the rate of formation of hydroxylated products of BaP (52). Mitochondrial protein (200 μg) and microsomal protein (200 μg) were incubated in 0.9 ml of BSA/potassium phosphate buffer (1 mg/ml BSA in 0.10 M potassium phosphate buffer, pH 7.4) along with 25 μl of NADPH (10 mM). Mitochondrial protein was reconstituted with 0.2 nmol of purified Adx and 0.02 nmol of NADPH-Adx reductase (AdxR) to compensate for the loss of Adx and other soluble proteins during mitochondrial isolation as reported before (35). The assay was started with the addition of 2 mM BaP and incubating the reaction mixture at 37 °C for 20 min. The reaction was stopped by addition of a 2:1 mixture of hexane/acetone (v/v). The enzyme blank consisted of hexane/acetone added before the addition of BaP but with mitochondrial protein added later. The upper organic phase was removed and extracted with 1.5 ml of 1 N NaOH. The aqueous alkaline phase was used for fluorescence measurement (396 nm excitation and 522 nm emission) using a Photon Technology International fluorometer. The activity (nmol of BaP hydroxylated/mg of protein/min) was calculated using the formula (nmol/min/mg = FU/min/mg × 623/2062), where FU is fluorescence units. All reactions were carried out in triplicate.

Measurement of Cytochrome P450 Content—The P450 contents of mitochondrial and microsome membranes were measured by the dithionite-CO difference spectra as described by Omura and Sato (53) and as modified (54) using a dual-beam spectrophotometer (Cary 1E; Varian, Walnut Creek, CA). The spectrum was recorded over the range of 400–500 nm. The P450 contents were calculated as described (53).

In Vitro Transport of Protein into Isolated Mitochondria—The use of rat liver mitochondria is the preferred system for protein import because of the ease of isolating functionally intact mitochondria, and also proteins from diverse cell and tissue types can be imported efficiently. *In vitro* protein import was carried out using ^{35}S-labeled proteins in isolated rat liver mitochondria essentially as described before (37). Treatment of mitochondria with trypsin (150 μg/mg mitochondrial protein) was carried out for 20 min on ice. Control mitochondria were incubated similarly without added trypsin. Soybean trypsin inhibitor (1.5 mg/mg protein) was added to all samples to terminate the reactions. Mitochondria were re-isolated by pelleting through 0.8 M sucrose, and the proteins were subjected to SDS-PAGE followed by fluorography.

ROS Production—Intracellular generation of ROS was measured using the fluorogenic probe 2,7-dicholorofluorescin diacetate as described elsewhere (55). ROS generation with isolated mitochondria and microsomes was also measured using the procedure described before (55). The cells and mitochondria were also treated with membrane-permeable catalase and SOD as controls. Cellular fluorescence was membrane-permeable and then measured using a fluorescence plate reader with excitation/emission filters suitable for fluorescence (480/535 nm).

Mitochondrial Respiratory Complex Activities—Mitochondrial respiratory complex activities were measured as described before (56). Briefly, the complex I activity was recorded as decreasing absorption at 340 nm (NADH oxidation) of reaction mixtures containing 200 μM NADH and 100 μM ubiquinone-1, in the presence of 1.5 mM KCN, and the rotenone-sensitive activity was calculated. The activity of CcO was measured spectrophotometrically by following the oxidation of ferrocytochrome *c* at 550 nm. The standard assay mixture contained the following: 0.25 M sucrose, 50 mM Tris-HCl, pH 8.0, 0.2 mM potassium EDTA, and mitochondria (~10 μg of protein/ml).

Immunofluorescence Microscopy—Immunofluorescence microscopy was carried out with methanol-fixed cells permeabilized using 0.1% Triton X-100 (v/v) essentially as described previously (57) using primary CYP1B1 (anti-rabbit) and CcOI (anti-mouse) antibody at 1:100 dilutions (v/v) each. The cells were then stained with 1:100 dilutions (v/v) of Alexa 488-conjugated anti-rabbit antibody and Alexa 594-conjugated anti-mouse IgG (Molecular Probes, Eugene, OR). Slides were viewed through a Leica TCS SP5 confocal microscope, and the Pearson's coefficient for colocalization was calculated using Volocity software 4.0.

Immunogold Electron Microscopy—Mitochondria were isolated as described above, and the trypsin-treated mitochondria from control and CYP1B1-transfected cells were fixed in 5% glutaraldehyde (v/v). Mitochondria were dehydrated through a graded ethanol series and embedded in hard grade LR White Resin (Sigma). The sections were then examined and photographed using a JEOL (Hammarbaccan, Sollen Tuna, Sweden) 100CX electron microscope.

shRNA-mediated Gene Knockdown and Stable Cell Generation—The 29-nucleotide short hairpin oligonucleotides (four constructs each for ADX and NPR), cloned in retroviral GFP vectors (pGFP-V-RS), were obtained from Origene (Rockville, MD) and evaluated for efficiency by transient transfections in A549 cells for 48 h. The most effective shRNA constructs (ADX, TGATGGTGAAACATTAACAACCAAAGGAA, and NPR, CAGAACACCTTCTACGACATCGTGGCTGA) were used to generate retroviral particles and further transduced in A549 cells as described before for obtaining stable cells. A plasmid containing a scrambled shRNA sequence and vector alone plasmid served as the negative controls. The positive clones were selected using medium containing 90% DMEM, 10% FBS, 1% penicillin/streptomycin (v/v), and puromycin (6 μg/ml). Adx and NPR protein and mRNA levels in isolated clones were determined by Western blotting and real time PCR, respectively.

mRNA Quantification by Real Time PCR—Total RNA was isolated from cells grown to confluence with the use of TRIzol reagent (Invitrogen), and the concentration of RNA was determined spectrophotometrically with the use of a Nanodrop instrument (Thermo Fisher Scientific, Waltham, MA). RT-PCR was carried out with reverse transcriptase (Applied Biosystems) and quantified on an Applied Biosystems 7300 instrument using gene-specific primer sets. Dissociation curves were established for each polymerase chain reaction product. The detection and quantitation of nucleic acid levels were done using inbuilt software with β-actin as the reference gene.

Long Amplicon Quantitative PCR of Mitochondrial (mt) DNA—Long amplicon quantitative PCR is a method that indirectly measures general structural DNA damage. It is based on the principle that the DNA templates with oxidative damage or chemical modifications hinder the DNA polymerase activity and, as a consequence, serve as a poor template for amplification. Quantification of amplification product allows one to evaluate the extent of oxidative damage in the target genome. Quantitative PCR was performed as described previously (58). Briefly, 50 ng of DNA was amplified with rTth DNA polymerase (Applied Biosystems, Foster City, CA) using primers for mitochondrial and nuclear targets. Small mitochondrial and nuclear DNA targets were amplified as control. The primer nucleotide sequences were as follows: for the 17.7-kb 5′-flanking region of the β-globin gene (GenBank™ database accession number J00179), 5′-TTGAGACGCATGAGACGTGCAG-3′ (RH1024) and 5′-GCACTGGCTTAGGAGTTGGACT-3′ (RH1053); and for the 16.2-kb fragment of the mitochondrial genome, 5′-TGAGGCCAAATATCATTCTGAGGGGC-3′ (RH1065) and 5′-TTTCATCATGCGGAGATGTTGGATGG-3′ (RH1066). The DNA amplicons were analyzed on 0.6% agarose gels.

Statistical Analysis—Means ± S.D. values were calculated from three to five independent experiments. Statistical significance (p values) between control and experimental or paired experiments was calculated using the Student's t test. A p value of 0.05 (*) was considered significant, and 0.001 (**) was considered highly significant.

RESULTS

BaP-induced CYP1B1 in Mitochondria—MCF-7 cells, known to respond to the Ahr agonists BaP and TCDD, were used to investigate the possible mitochondrial localization of CYP1B1 and its potential role in inducing cellular toxicity. The mitochondrial and microsomal distribution of CYP1B1 and CYP1A1 in cells treated with BaP (20 μM) for 48 and 72 h is shown in Fig. 1*A*. A marked increase in CYP1B1 and CYP1A1 proteins in both the mitochondrial and microsomal fractions was seen in cells treated with BaP but not in cells treated with the vehicle DMSO. The blot was also co-developed with antibodies to the microsomal marker NPR and mitochondrial marker Tom20 to assess the levels of cross-contamination. The immunoblots show that these mitochondria contained very low levels of NPR and that the microsomes contained low levels of Tom20 protein, indicating the relative purity of the cell fractions used.

Measurement of mitochondrial respiration using a Seahorse flux analyzer showed (Fig. 1*B*) that BaP treatment adversely affected the ATP-coupled, maximum-uncoupled, and reserve respiration in MCF-7 cells. Notably, TMS (a specific and selective inhibitor of CYP1B1) nearly completely reversed the BaP-induced respiratory impairment, suggesting the possible role of CYP1B1 in this inhibition.

To assess the possible cause of mitochondrial damage, we measured the AHH activity of mitochondria and microsomes from treated and untreated cells. Mitochondrial AHH activity was induced >10-fold (specific activity 474) in cells treated with BaP for 48 h, which steadily declined to 229 and 168 by 72

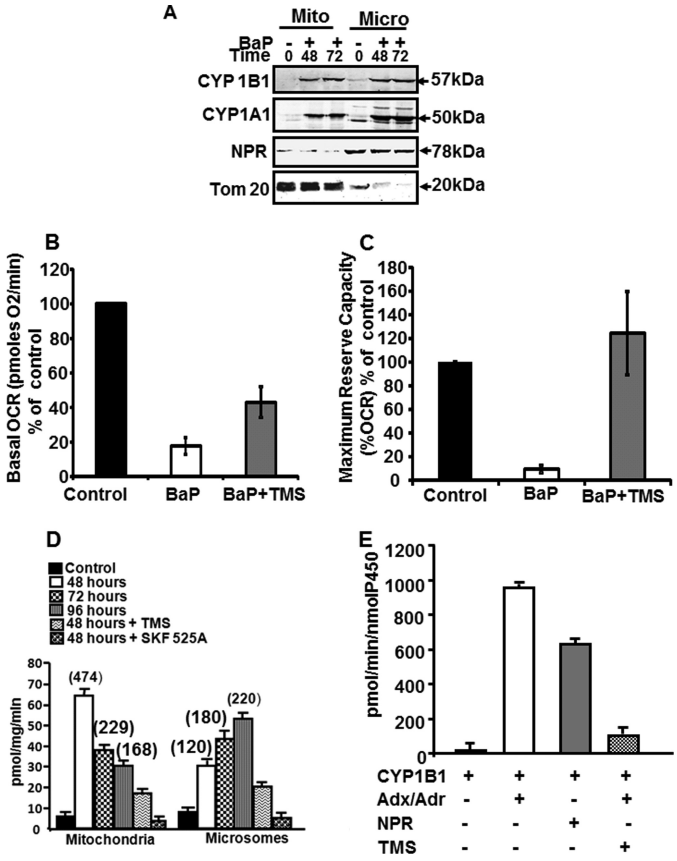

FIGURE 1. **Induction of CYP1B1 and mitochondrial dysfunctions in MCF-7 cells exposed to BaP.** *A*, induction of CYP1B1 in the mitochondria (*Mito*) and microsomes (*Micro*) isolated from MCF-7 cells treated with BaP (20 μM) for 48 or 72 h or with DMSO alone. Mitochondrial and microsomal proteins (50 μg) each were resolved by SDS-PAGE and subjected to immunoblot analysis with CYP1B1 antibody (1:1500, v/v) and CYP1A1 antibody (1:4000, v/v). The blot was also codeveloped with NPR (1:2500, v/v) and Tom20 (1:2000, v/v) antibodies to assess levels of cross-contamination. *B* and *C*, rate of O_2 consumption (*OCR*) was measured using a Seahorse Bioscience XF24 Extracellular Flux Analyzer. Cells (50,000) from control, BaP treatment (20 μM), and TMS + BaP were cultured in DMEM/F-12 medium for 72 h followed by a change with XF medium (low buffered and bicarbonate-free, pH 7.4) for 1 h before the assay. TMS was used at a concentration of 0.8 μg/ml. The plate was incubated without CO_2 for 1 h before recording the respiration rates. Oligomycin (2 μg/ml), 2,4-dinitrophenol (75 μM), and rotenone (1 μM) were injected through ports A, B, and C, respectively. Basal OCR (pmol of O_2/min) and maximum reserve capacity (%OCR) were analyzed using XF software. *D*, BaP hydroxylation activity (AHH) was assayed using MCF-7 cells treated with 20 μM BaP for 48, 72, and 96 h. Digitonin-treated mitochondria and microsomes (200 μg of protein each) were incubated and used for assaying AHH activity as described under "Experimental Procedures." The values in *parentheses* show specific activity (pmol of product formed/nmol of CYP/min). *E*, bacterially expressed and purified human CYP1B1 (0.2 nmol of CYP) was assayed for AHH activity by reconstituting with 0.5 nmol of NPR (along with phospholipid vesicles) and Adx + AdxR as described under "Experimental Procedures." TMS was added at a concentration of 10 μg/ml to study the reaction specificity. The means ± S.D. were calculated from three independent measurements.

and 96 h, respectively (Fig. 1*C*). The activity in the microsomal fraction was induced by about 3-fold (specific activity 120) at 48 h, which steadily increased to 180 and 220 by 72 and 96 h, respectively. The basis for the distinctive activity patterns in the two membrane compartments remains unclear, although different rates of induction of CYP1 enzymes may be a factor. Both mitochondrial and microsomal AHH activities were inhibited by about 90% by SKF525A, a general inhibitor of all CYPs. However, TMS, a specific and selective inhibitor of CYP1B1, inhibited the mitochondrial AHH activity by about 75% as opposed to 24% inhibition of the microsomal fraction. In keeping with our previous results with purified mitochondrial enzyme and transgenic knock-in system (59, 60), these results suggest a relatively high CYP1B1 contribution to the mitochondrial AHH activity. This possibility was further verified by *in vitro* reconstitution of AHH activity using purified CYP1B1. CYP1B1 reconstituted with Adx and AdxR showed about 1 nmol/nmol of P450/min compared with 0.7 nmol/nmol of P450/min when reconstituted with NPR. The latter was reconstituted in phospholipid vesicles. TMS nearly completely inhibited the activity confirming the role of CYP1B1-dependent metabolism. These results show that BaP treatment affects mitochondrial function possibly through CYP1B1-mediated AHH activity.

Mitochondrial Targeting of CYP1B1—A combination of N-terminal progressive deletion of the protein and import of *in vitro* translated ^{35}S-labeled proteins into isolated rat liver mitochondria was used to study mitochondrial targeting. Different N-terminal truncated constructs (full-length CYP1B1, + 34, + 54, and + 141) were used for the *in vitro* import assay to locate the signal sequence responsible for translocation of CYP1B1 inside mitochondria (Fig. 2*A*). Analysis of the N-terminal 140 amino acid sequence of human CYP1B1 indicated a strong mitochondrial targeting signal in the region of +34 to +54. Fig. 2*B* shows the translational efficiencies of WT, +34, +54, and +141 cDNA constructs. WT protein was imported with a relatively lower efficiency, as indicated by the trypsin-resistant fraction (Fig. 2*C*). The +34 protein was imported at the highest efficiency, although the +54 and +141 proteins were imported very poorly. Notably, the imported (trypsin resistant) proteins, in the case of both WT and +34, were of nearly similar in size to the respective input proteins, suggesting no import-linked mitochondrial processing. Fig. 2*D* shows the import efficiency of a cytosolic protein, DHFR and DHFR fused to yeast ATPase 6 import signal (Su9-DHFR), which is cleavable by the matrix protease. This control experiment shows that Su9-DHFR was imported at high efficiency and that the signal was cleaved as indicated by the size of the trypsin-protected protein. DHFR alone, however, was not imported at a significant level. These results suggest that the mitochondrial import signal of CYP1B1 probably resides between +34 and +54 amino acids of the sequence.

Previously (using both stable and transient expression systems), we showed that mitochondrial CYP1A1 was N-terminally truncated (32, 35, 37, 44). Analysis of mitochondrial and microsomal proteins from COS-7 cells transfected with WT CYP1B1 by SDS-PAGE showed no detectable difference in their migration rates. However, analysis by high resolution Tricine gel electrophoresis showed a marginal difference between

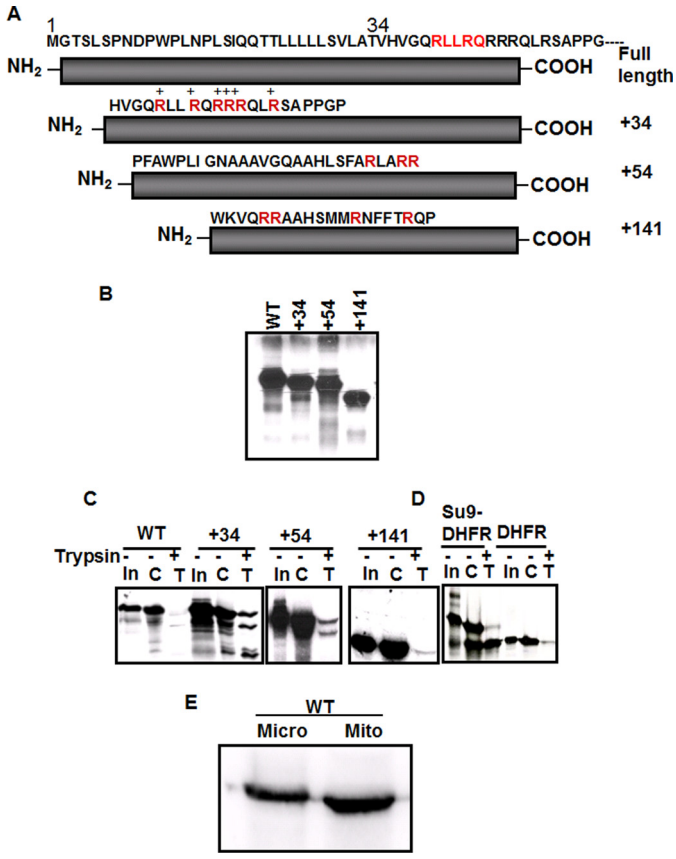

FIGURE 2. **Localization of mitochondria targeting signal of CYP1B1.** *A*, cDNA constructs used for *in vitro* import studies. Full-length CYP1B1 and other mutants (+34, +54, +141) were cloned in PCDNA3.1 and PCMV4 for *in vitro* transcription-linked translation and cell transfection, respectively. *B*, ^{35}S-labeled translation products of WT CYP1B1, +34, +54, +141 1B1 cloned in PCDNA3.1. *C*, import of ^{35}S-labeled translation products in isolated rat liver mitochondria. *D*, DHFR and Su-9 DHFR, in which the pre-sequence of subunit 9 of *Neurospora crassa* F_0F_1-ATPase was fused to DHFR used as negative and positive controls, respectively. In all experiments, trypsin digestion (150 μg/ml) of mitochondria was performed for 20 min on ice. Proteins (50 μg each) were subjected to SDS-PAGE and fluorography. *C* on the top of lanes represents control experiments in which total protein bound and imported into mitochondria is present; *T* represents trypsin-treated mitochondria in which only the protein imported into mitochondria is present. In the lanes marked *In*, 10% of the counts used as input for the import reactions were loaded. *E*, patterns of mitochondrial and microsomal CYP1B1 in COS-7 cells transfected with WT CYP1B1 cDNA for 48 h. Fifty μg of protein each was loaded onto a 12% Tricine gel (w/v), and proteins were probed with CYP1B1 antibody (1:1500, v/v).

the microsomal and mitochondrial CYP1B1 forms, with the latter migrating faster (Fig. 2*E*).

The possible role of the sequence region 34–54 of CYP1B1 in mitochondrial transport was ascertained using transient transfection of cDNA constructs in COS-7 cells. In almost all CYPs bimodally transported to mitochondria, a stretch of positively charged residues immediately upstream of the transmembrane domain has been shown to be important for signal activity (31, 61). With a view of localizing the mitochondrial targeting signal of CYP1B1, we substituted Arg residues with Ala between amino acid sequence positions 41–48. The two mutant cDNAs (Rmut1 and Rmut2) and WT cDNA, as shown in Fig. 3*A*, were transfected in COS-7 cells, and the protein content in the mitochondrial and microsomal fractions was analyzed by immunoblot analysis. As shown in Fig. 3*B*, cells transfected with WT cDNA for 48 h showed a higher CYP1B1 protein level in mito-

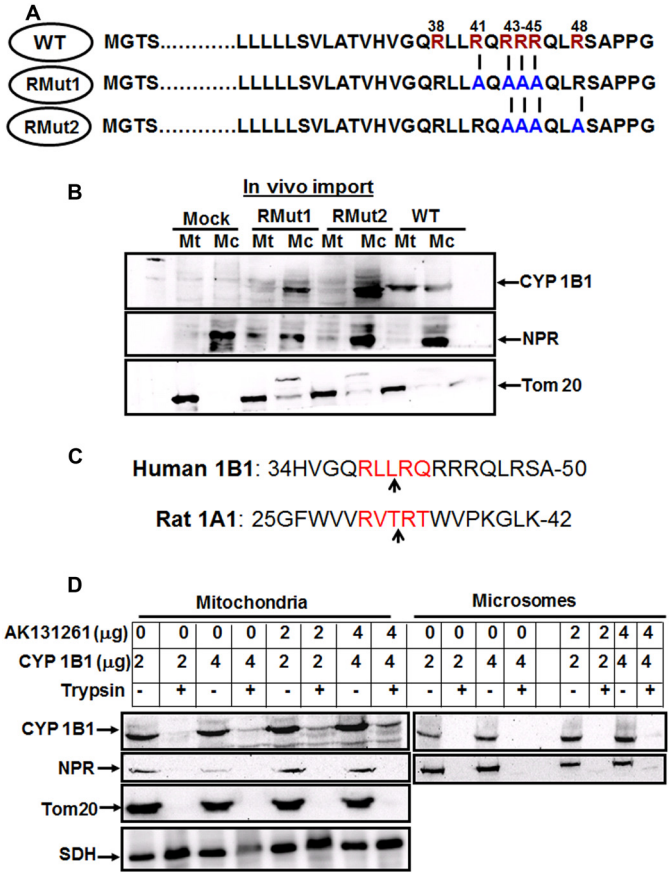

FIGURE 3. **Putative mitochondrial targeting signal of CYP1B1 and endoprotease-processing site.** *A*, sequence of putative mitochondrial signal region (*WT*) and two mutant versions (*RMut1* and *RMut2*) are shown. *B*, *in vivo* targeting patterns of WT and Mut proteins in cells transfected with respective cDNA constructs. Proteins (50 μg each) were resolved on SDS-PAGE and subjected to immunoblot analysis with CYP1B1 antibody (1:1500, v/v). The blot was also codeveloped with NPR (1:2500, v/v) and TOM20 (1: 2000, v/v) antibodies to detect any cross-contamination. *C*, conservation of putative Ser protease cleavage site in the N-terminal signal region of CYP1B1. The Ser protease cleavage site of CYP1A1 was used for comparison. *D*, COS-7 cells were cotransfected with varying amounts of full-length CYP1B1 and AK131261 cDNA. Mitochondria (*Mt*) and microsomes (*Mc*) were isolated as described under the "Experimental Procedures" and subjected to trypsin digestion (100 μg of trypsin/mg of protein for 20 min on ice). An equal amount of protein (50 μg each) was loaded onto SDS-PAGE and subjected to immunoblot analysis with CYP1B1 antibody. The blots were also probed for NPR, an ER-specific marker: Tom20, an outer mitochondrial membrane marker, and SDH, an inner mitochondrial membrane-specific marker protein.

chondria than in the microsomal fraction. In the case of Rmut1 protein, a minor component is detected in the mitochondria, although a more robust level is seen in the microsome fraction. With the Rmut2 protein, a substantially higher level of CYP1B1 was seen in the microsomes, although the mitochondrial level was very low. These results suggest that the mitochondrial targeting signal lies within the Arg clusters from sequence positions 41–48, as proposed in our bimodal targeting hypothesis (31, 61). Increasing the hydrophobicity of the chimeric signal region markedly increases the ER targeting efficiency of the protein (35).

Previously, we showed that activation of a cryptic mitochondrial signal of nascent mouse and rat CYP1A1 required sequence-specific processing at residue 32 by a cytosolic Ser protease (32, 35, 37, 44). The human CYP1B1 also contains a putative Ser protease cleavage site, similar to the rat CYP1A1 site, between residues 38 and 42 of the protein (Fig. 3*C*). We therefore tested the effects of cotransfection with intact CYP1B1 encoding cDNA and cDNA encoding the catalytically active 50-kDa derivative of polyserase 1 (AK131261). Immunoblot analysis of mitochondria and microsomes from transfected cells (Fig. 3*D*) showed that co-transfection with increasing concentrations of AK131261 construct (0–4 μg) steadily increased the level of trypsin-resistant CYP1B1. The microsomal CYP1B1 under these conditions was completely degraded by trypsin. The results also showed low levels of NPR in the mitochondrial isolates, which were completely degraded by trypsin. As expected, TOM 20 protein (with an outer membrane extrinsic region) was degraded. However, SDH, an inner membrane protein facing the matrix side, was resistant to trypsin. These results suggest that coexpression with Ser protease increased mitochondrial targeting of CYP1B1.

Mitochondrial localization of WT and +34CYP1B1 was also ascertained by immunofluorescence confocal microscopy and immunogold electron microscopy. COS-7 cells were transfected with the indicated cDNAs and stained with antibody against CYP1B1 and antibody to the mitochondrial genome-encoded CcOI subunit (Fig. 4*A*). As expected, mock-transfected cells were not stained to a significant level by CYP1B1 antibody. Cells transfected with WT CYP1B1 showed immunoreactivity with the CYP1B1 antibody, part of which overlapped with CcO antibody-stained structures. Cotransfection of cells with CYP1B1 cDNA along with AK131261 cDNA significantly increased overlapping staining with CcO antibody, as indicated by a Pearson's coefficient of 0.72. Transfection with +34CYP1B1 cDNA gave a robust CYP1B1 expression and also higher level of colocalization with mitochondrial CcOI antibody Pearson's coefficient of 0.80.

Immunogold analysis of isolated mitochondria from mock-transfected and cells transfected with WT CYP1B1 are shown in Fig. 4*B*. Mitochondria from CYP1B1-transfected cells showed a high number of electron dense particles, indicating intramitochondrial localization. Immunoblotting revealed the levels of alkaline Na_2CO_3 extractable (soluble) and resistant (pellet) CYP1B1 in the mitochondrial and microsomal fractions of transfected cells (Fig. 4*C*). CYP1B1 from mitochondrial fractions of cells transfected with WT and +34CYP1B1 constructs were nearly quantitatively extracted with alkaline Na_2CO_3 suggesting a membrane extrinsic topology, whereas the CYP1B1 associated with the microsomal fraction was completely resistant to Na_2CO_3 extraction, suggesting transmembrane topology.

Endoproteolytic Processing of CYP1B1—The possible processing of CYP1B1 by a cytosolic protease is difficult to assess by a change in electrophoretic mobility because the parent and processed proteins migrate very closely to each other, even on Tricine gels. To firmly establish the N-terminal processing, we fused DHFR to the N terminus of CYP1B1 (Fig. 5*A*) such that the processed components can be easily resolved by gel electrophoresis. Because the processing enzyme is in the cytoplasm, the level of processing directly correlates with the level of 57-kDa CYP1B1 in mitochondria. Fig. 5*B* shows the immunoblot of total cell extract of COS-7 cells transfected with empty

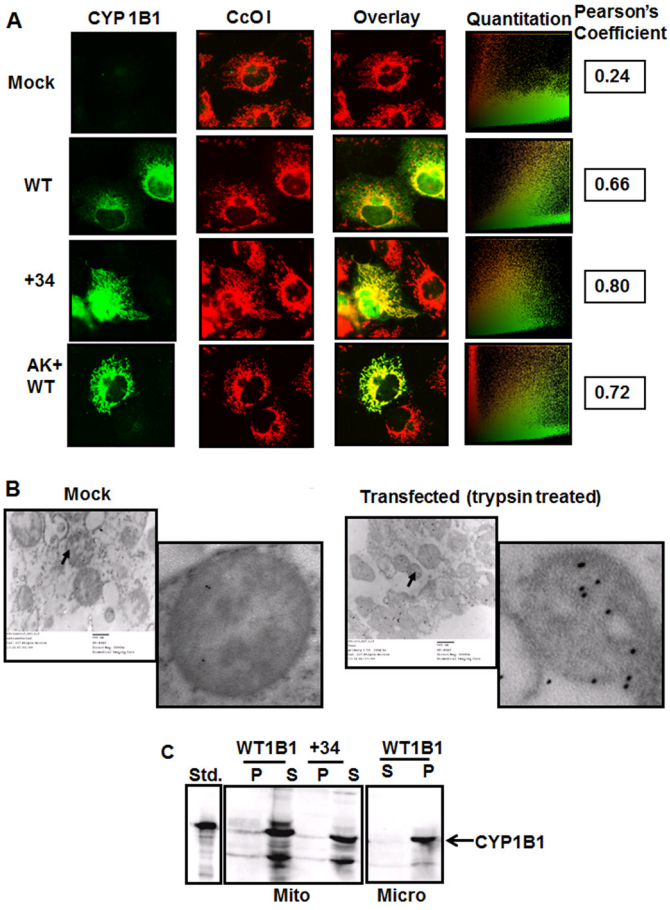

FIGURE 4. **Intramitochondrial localization of CYP1B1 by immunofluorescence and immunogold electron microscopy.** *A*, COS-7 cells grown on coverslips were transfected with vector alone, WT, + 34 CYP1B1 cDNAs, and in one case cotransfected with AK131261 cDNA for 48 h. The cells were fixed with chilled methanol, and cells were double-immunostained with antibodies specific for CYP1B1 and CcOI. The stained patterns were overlaid, and the Pearson's coefficient for each overlay was calculated based on the scatterplot using Volocity software. *B*, COS-7 cells were transfected with vector and WT CYP1B1, and the trypsin-digested mitochondrial pellets were used for immunogold electron microscopy. The sections were stained with antibody to CYP1B1 and costained with gold-conjugated (10 nm gold particles) secondary antibody. *C*, solubility of mitochondrial and microsomal CYP1B1 in alkaline Na_2CO_3. Mitochondria and microsomes from +34CYP1B1 or WT CYP1B1 cDNA-transfected COS-7 cells were extracted with 0.10 M Na_2CO_3, pH 11.0. The total soluble protein (*S*) and proteins from the insoluble membrane fraction (*P*) were isolated and resolved by SDS-PAGE and subjected to immunoblot analysis using CYP1B1 antibody.

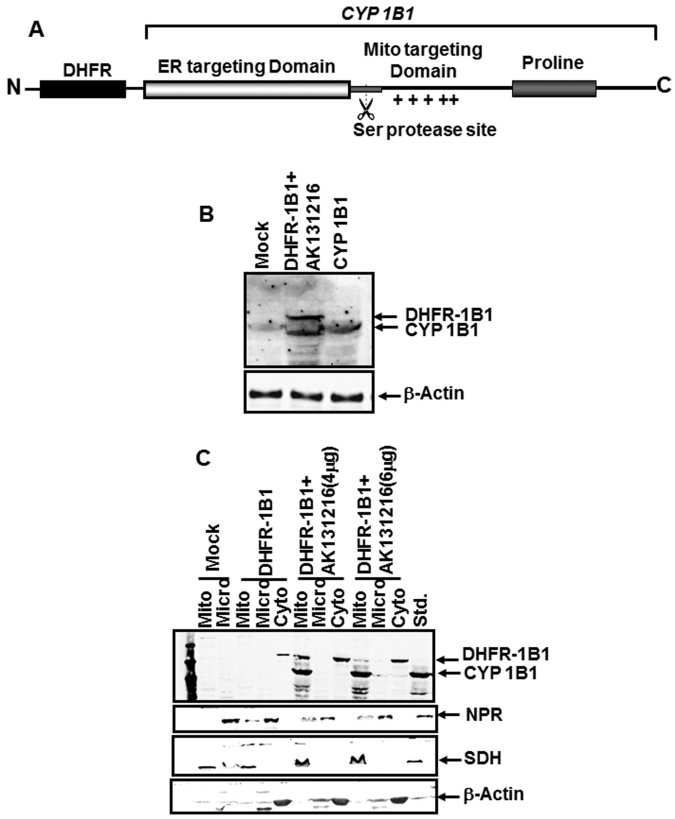

FIGURE 5. **Endoproteolytic processing at the N-terminal signal region of human CYP1B1 protein.** *A*, fusion construct of DHFR fused to the N terminus of CYP1B1 was generated as described under the "Experimental Procedures." The position of DHFR, various signal domains of CYP1B1, and the putative processing sites are shown. *B*, COS-7 cells were transfected with mock, WT CYP1B1, or DHFR-1B1 cDNAs with or without AK131261 cDNA as indicated. Total cell extracts (50 μg of protein each) were loaded on SDS-PAGE, and the immunoblot was developed with CYP1B1 antibody. The blot was also developed with actin antibody to assess loading levels. *C*, subcellular distribution of fusion protein and processed product. COS-7 cells were transfected with mock, DHFR-1B1, and with varying amounts of AK131261 cDNA as described in *B*. Mitochondria (*Mito*), cytosol (*Cyto*), and microsomes (*Micro*) were isolated from transfected cells, and 50 μg of protein each was subjected to immunoblot analysis using CYP1B1 antibody (1:1500, v/v). The same blot was also developed with NPR, SDH, and β-actin antibodies. *Std.*, standard.

vector, DHFR-CYP1B1 fusion construct, plus the AK131261 cDNA and WT CYP1B1 cDNA. DHFR-1B1-transfected cells show parent unprocessed fusion protein and also a faster migrating processed protein. The processed protein showed a minor difference in migration compared with the WT CYP1B1, possibly because of the 30–40-amino acid difference in size between the processed and unprocessed protein. The mitochondrial, microsomal, and cytoplasmic distribution of DHFR-1B1 and processed CYP1B1 in cells transfected with or without the AK131261 cDNA are shown in Fig. 5*C*. The mitochondrial and microsomal fractions of cells transfected with DHFR-1B1 cDNA alone did not contain any detectable protein. The cytoplasmic fraction contained a minor amount of full-length protein suggesting that the fusion protein is probably turned over more rapidly in these cells. Cells co-transfected with AK131261 cDNA show significant unprocessed protein associated with mitochondria and cytoplasm. The mitochondrial fraction also contained processed CYP1B1, suggesting that protease processed CYP1B1 is targeted to mitochondria. As shown later, this faster migrating component was resistant to limited trypsin treatment. Transfection with a higher amount (6 μg) of AK131261 cDNA markedly reduced the level of unprocessed fusion protein associated with both mitochondria and cytoplasm. These results suggest that, similar to that reported for CYP1A1, an endoprotease processing activates the mitochondrial targeting signal.

The possible endoprotease processing site between sequences 37 and 42 was verified by Ala scan mutations. Ala substitutions at 37, 38 (designated as M1), 38, 39 (designated as M2), 39, 40 (designated as M3), and 40, 41 (designated as M4) were introduced in both CYP1B1 cDNA and DHFR-1B1 cDNA constructs (Fig. 6*A*). The WT and mutant CYP1B1 constructs (6 μg) were transfected along with the AK131261 cDNA construct (4 μg of DNA), and the mitochondrial and microsomal

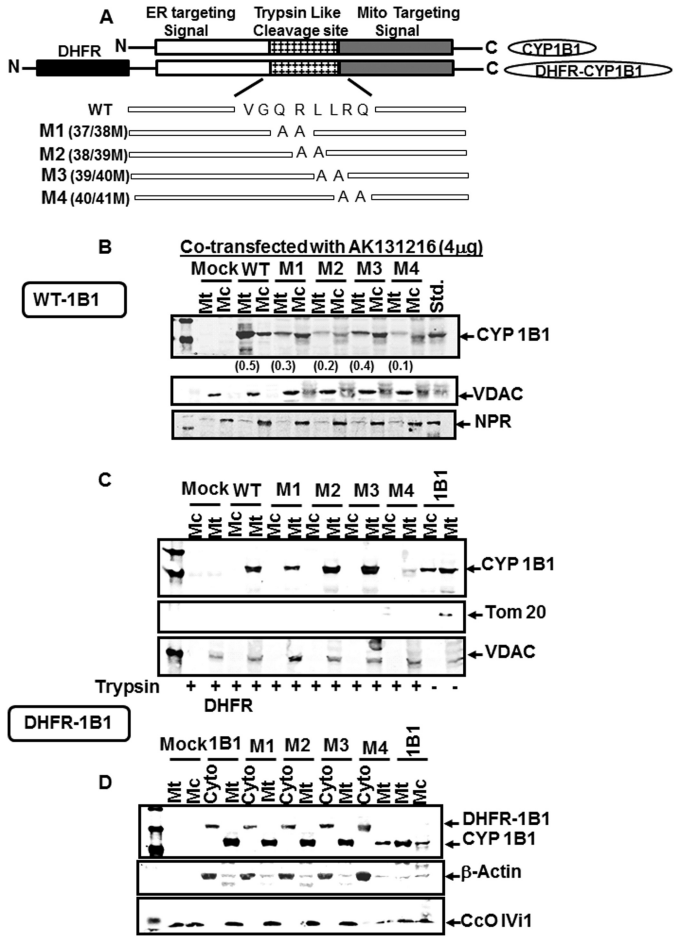

FIGURE 6. **Sequence specificity of processing by the endoprotease.** *A*, predicted processing sites and sequence of WT CYP1B1 and DHFR-1B1 and alanine scan mutations are shown. Constructs where amino acids at positions 37/38, 38/39, 39/40, and 40/41 were mutated to alanines were designated as M1, M2, M3 and M4, respectively. *B*, processing of WT and mutant (*M1–M4*) CYP1B1 protein cotransfected with 4 μg of AK131261 cDNA in COS-7 cells. Mitochondrial and microsomal samples (50 μg each) were subjected to immunoblot analysis. The *numbers* below the blot in *parentheses* indicate relative band intensities of mitochondrial CYP1B1 protein. *C*, experiment was performed similar to that in *B* except that mitochondria and microsomes were treated with trypsin (100 μg/mg at 4 °C for 20 min). *D*, DHFR-1B1 fusion constructs and Ala scan mutant constructs were cotransfected with 4 μg of AK131261 cDNA in COS cells. Mitochondrial (*Mito*), microsomal (*Micro*), and cytosolic (*Cyto*) proteins (50 μg per lane) were subjected to immunoblot analysis with CYP1B1 antibody to detect the levels of precursor and processed protein. The blot was also codeveloped with antibody to β-actin and CcO IVi1 to detect the level of cytosolic contamination of mitochondrial isolates. *Std*, standard.

fractions were analyzed by immunoblot analysis using CYP1B1 antibody. The level of mitochondrial CYP1B1 protein was marginally reduced in the case of Mut1 protein (R37A/R38A) and markedly reduced with Mut4 protein (R40A/R41A) (Fig. 6*B*). The mitochondrial isolates were relatively free of microsomal contamination, as evidenced by the low levels of NPR. Fig. 6*C* presents a similar experiment except that all samples, excepting the two control samples, were treated with trypsin. Clearly the microsomal CYP1B1 in all samples was degraded, although the mitochondrial CYP1B1 was resistant, indicating an intra-mitochondrial location. As in the previous experiment, the M1 construct yielded a marginal reduction in mitochondrial CYP1B1 content, whereas M4 showed marked reduction in mitochondrial content. Immunoblots of fractions from cell transfection experiments carried out with DHFR-1B1 fusion constructs revealed that the slower migrating DHFR-1B1 fusion protein was mostly in the cytosolic fractions of all transfected cells (Fig. 6*D*). The mitochondrial fractions of cells transfected with WT protein and M1, M2, and M3 showed similar levels of mitochondrial, putative processed protein. The M4 construct, however, yielded a markedly lower level of processed mitochondrial protein. These results together confirm that nascent CYP1B1 protein is processed by the cytosolic endoprotease that is also known to be induced by β-naphthoflavone and other Ahr agonists (32), and that the processing site resides between sequence 37 and 42 of the protein.

Distinctive Patterns of CYP1 Gene Expression and Protein Levels in Transgenic Knock-out Mice—Because of the small size of the mouse mammary tissue, *in vivo* effects on AHH on mitochondrial function were studied in the lung tissue. The levels of CYP1 mRNA and proteins in the lungs of WT, *Cyp1a1/1a2*-null, and *Cyp1b1*-null mice were measured, in response to TCDD or BaP treatments. *Cyp1b1* mRNA levels in WT and *Cyp1b1*-null mice were measured by exon 3 region primers that discriminate between the WT transcripts and transcripts from PGK-Neo knock-in sequence that disrupts the gene (21). *Cyp1a1* and *-1a2* mRNA levels were measured in WT and *Cyp1a1/1a2*-null mice as described before (62). Both TCDD and BaP induced CYP1B1 mRNA by 17–20-fold in lungs of WT mice but not of *Cyp1b1*-null mice (Fig. 7, *A* and *D*). Notably, lungs of *Cyp1a1/1a2*-null mice expressed a nearly 60-fold higher level of *Cyp1B1* mRNA, which was increased to nearly 400-fold by treatment with BaP. Similarly, *Cyp1a1* and *-1a2* mRNAs were induced 10–20-fold in WT mice but not in *Cyp1a1/1a2*-null mice. However, *Cyp1a1/1a2*-null mice expressed 60–80-fold higher *Cyp1a1* and *-1a2* mRNA levels in *Cyp1b1*-null mice, which were increased to about 400-fold by BaP administration. Although nearly 400-fold induction of mRNA was surprising, previous studies reported induction from 0.003 to 80 mol of *Cyp1a1* mRNA relative to β-actin mRNA in *Cyp1a2*-null mice and a similar level of induction of *Cyp1a2* mRNA in *Cyp1a1*-null mice (62). In line with previous observations by Nebert and co-workers (62, 63), these results suggest a yet unknown intergenic negative regulation of expression of *Cyp1* family members.

The immunoblot in Fig. 7*E* shows that CYP1B1 protein level was induced markedly in both the mitochondrial and microsomal fractions of lungs from WT mice in response to BaP treatment. Consistent with the high mRNA levels, mitochondria and microsomes from untreated *Cyp1a1/1a2*-null mice showed relatively high CYP1B1 protein, which was markedly increased in the lungs of BaP-treated mice. Similar fractions from *Cyp1b1*-null mice failed to show significant CYP1B1 protein levels. CYP1A1 levels were also markedly increased in both the mitochondria and microsomes of WT mice as well as *Cyp1b1*-null mice following BaP treatment. Notably, despite the high levels of mRNA in *Cyp1b1*-null mice, the CYP1A1 protein levels were not high in uninduced controls. The reason for this apparent discrepancy remains unclear. Furthermore, *Cyp1a1/1a2*-null mice did not show significant CYP1A1 protein in both treated and untreated controls. Most notably, the

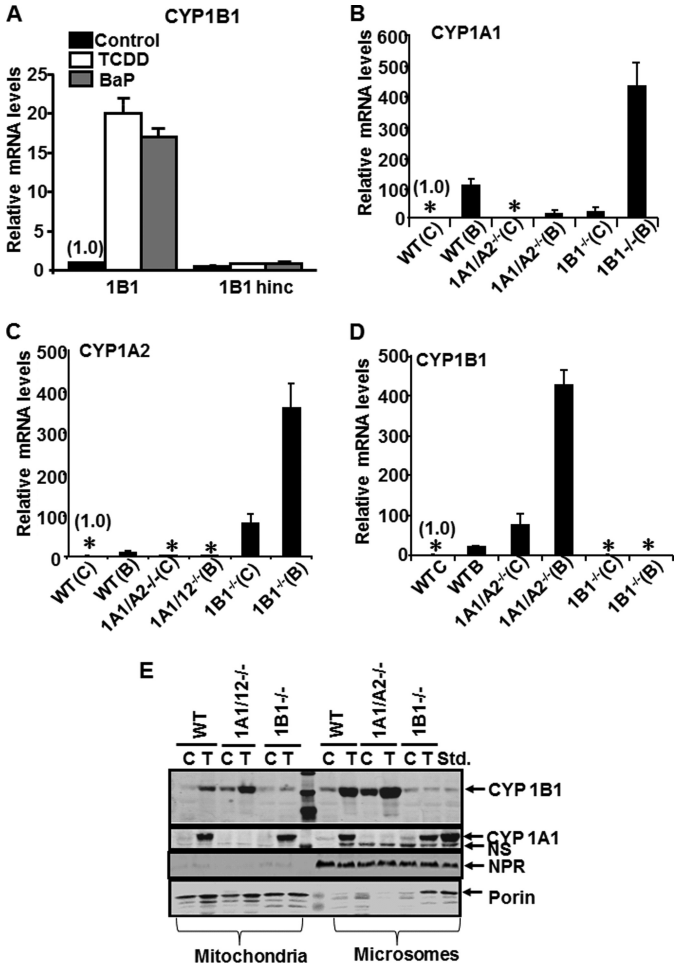

FIGURE 7. ***In vivo* induction of *Cyp1b1* mRNA and protein in WT, *Cyp1a1/1a2*-null, and *Cyp1b1*-null mice.** *A–D,* total RNA from control and treated lungs copied into cDNA was used for quantifying various *Cyp1* mRNAS as described under "Experimental Procedures." Means ± S.D. were calculated from three independent assays. *A*, *Cyp1B1* mRNA quantification in control and *Cyp1b1*-null mice. *B*, *Cyp1a1* mRNA quantified from WT, *Cyp1a1/1a2*-null, and *Cyp1b1*-null mice. *C*, *Cyp1a2* mRNA quantified from WT, *Cyp1a1/1a2*-null, and *Cyp1b1*-null mice. *D*, *Cyp1b1* mRNA quantification from WT, *Cyp1a1/1a2*-null, and *Cyp1b1*-null mice. *E*, mitochondria and microsomes isolated from lungs of control, BaP-, and TCDD-treated mice (50 μg of protein each) were subjected to immunoblot analysis using antibodies to CYP1B1 and CYP1A1. The membrane portions cut from the same blot were also developed with antibodies to NPR and porin to detect any cross-contamination. *, $p < 0.05$. *C*, control (untreated); *T*, treated; *NS*, nonspecific.

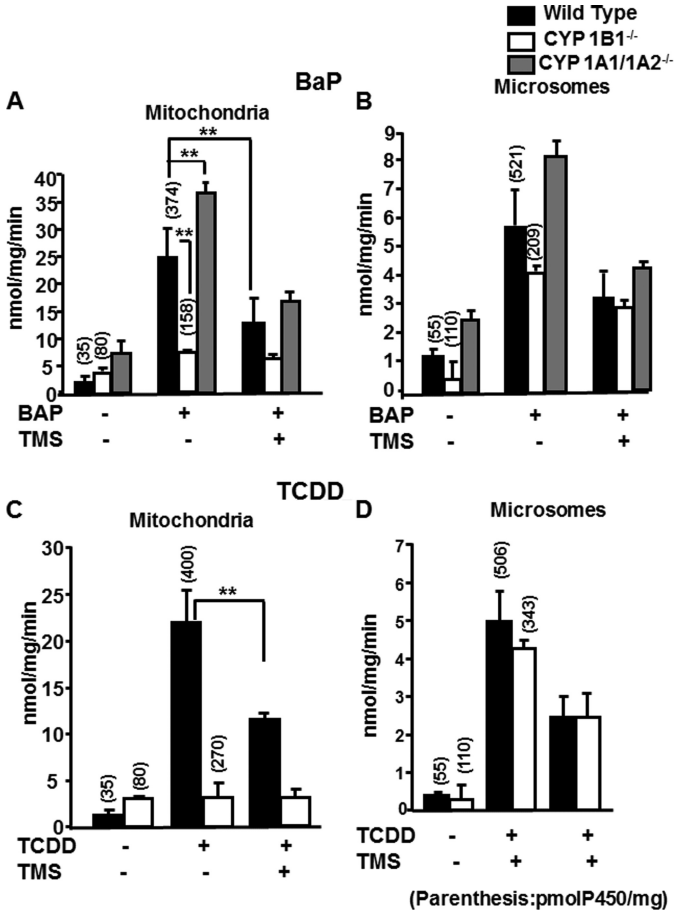

FIGURE 8. **Aryl hydrocarbon hydroxylase activity in the mitochondria and microsomes isolated from lungs of WT, *Cyp1a1/1a2*-null, and *Cyp1b1*-null mice.** *A* and *B*, mitochondrial and microsomal lung proteins (200 μg of protein each) from control and BaP-treated mice ($n = 6$) were used to determine the rates of benzo[*a*]pyrene hydroxylation as described under the "Experimental Procedures" and in Fig. 1. *C* and *D,* mitochondrial and microsomal protein (200 μg of protein each) from control and TCDD-treated mouse lungs was used to determine the rates of benzo[*a*]pyrene hydroxylation. Mitochondrial samples were reconstituted with Adx and Adr and the assays were carried out as detailed under the "Experimental Procedures." TMS (33 μM) was added at the start of the reaction. The activity was plotted as nanomoles of hydroxybenzopyrene formed per min/mg of protein for all groups. The *numbers in parentheses* over the bars represent CYP contents of mitochondria and microsomes from treated and untreated mouse lungs. Means ± S.E. were calculated from 4 to 6 independent assays. ** indicates $p < 0.001$.

400-fold induction of mRNAs in transgenic knock-out mice did not reflect in terms of protein levels possibly because of translational regulation or altered turnover rates. The mitochondrial fractions from treated and untreated lungs did not show significant NPR protein, and the microsomal fractions contained very low porin indicating the relative purity of subcellular fractions used.

Mitochondrial AHH Activity in Cyp1a1/1a2-null and Cyp1b1-null Mice—Mitochondria and microsomes from BaP- (Fig. 8, *A* and *B*) and TCDD (Fig. 8, *C* and *D*)-treated mice showed 10–15-fold induction of AHH activity in WT mice. The induction of AHH activity in *Cyp1b1*-null mice was very low in mitochondria but relatively high in the microsomes, possibly because of contributions from CYP1A1. As reported before (59, 60), mitochondrial CYP1A1 showed very low AHH activity when reconstituted with Adx and AdxR. Both mitochondria and microsomes from BaP-treated lungs from *Cyp1a1/1a2*-null mice showed AHH activity nearly 50–60% higher than the WT mice, consistent with the higher CYP1B1 protein levels in the lungs. TMS, a specific inhibitor of human CYP1B1, inhibited AHH activity by 50–60% in both mitochondria and microsomes from WT and *Cyp1a1/1a2*-null mice but not in *Cyp1b1*-null mice. Treatment with TCDD (Fig. 8, *C* and *D*) also induced the AHH activity in lung mitochondria and microsomes from the WT mice. There was no increase in mitochondrial AHH activity in *Cyp1b1*-null mice in response to TCDD; however, there was a substantial increase in activity in the microsomal fraction, possibly reflecting contribution from microsomal CYP1A1. TMS inhibited the mitochondrial and microsomal AHH activity by about 50% in the WT mice. However, the extent of inhibition with microsomes from *Cyp1b1-*

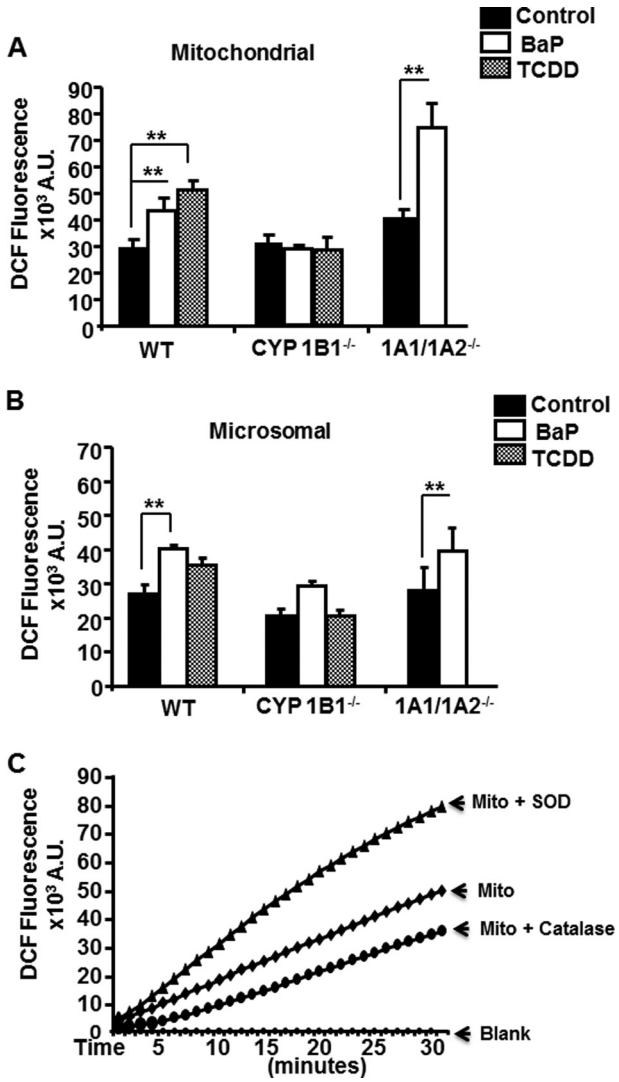

FIGURE 9. **ROS measurements in mitochondrial and microsomal isolates using the DCFH-DA method.** *A*, ROS levels in treated and untreated WT, *Cyp1a1/1a2*-null, and *Cyp1b1*-null mouse lung mitochondria (*Mito*). *B*, microsomes from treated and untreated WT, *Cyp1a1/1a2*-null, and *Cyp1b1*-null mouse lung were measured using DCFH-DA (5 μM). Details were as described under "Experimental Procedures." *C*, control experiment showing time-dependent increase of fluorescence using BaP-treated lung mitochondria from WT mice. Membrane-permeable catalase (10 units/ml) and SOD (30 units/ml) were added before the start of the reaction. The assays were run as described under the "Experimental Procedures" using 10 μg of brain cytosolic preparation per 200-μl reaction volume. The fluorescence was recorded at an excitation at 488 nm and emission at 525 nm for 15 min. **, $p < 0.001$.

null mice was only marginal. These results show that mitochondrial *Cyp1b1* is catalytically active in the metabolism of PAHs. In Fig. 8, *C* and *D*, the numbers in *parentheses* over the *bars* represent the Cyp contents (pmol of P450/mg of protein) of the samples as determined from their reduced CO difference spectra.

PAH-mediated Mitochondrial ROS Generation in Lungs of Cyp1a1/1a2-null and Cyp1b1-null Mice—The effects of BaP and TCDD on ROS generation in mitochondria from WT, *Cyp1a1/1a2*-null, and *Cyp1b1*-null mice was determined (Fig. 9) using DCFH-DA probe as described previously (55, 57). There was a significant increase in ROS production in both mitochondria and microsomes of WT mice treated with BaP or TCDD. However, there was no increase in ROS production in either cell compartment of *Cyp1b1*-null mice treated with either BaP or TCDD. Both of these agents, however, induced nearly 2-fold higher ROS in mitochondria and about 60% higher ROS in the microsomes of *Cyp1a1/1a2*-null mice. A control experiment showed the effects of membrane-permeable SOD and catalase on ROS production (Fig. 9*C*). Addition of SOD gave a much higher signal suggesting that mitochondria produced substantial $O_2^{\cdot-}$, which is converted to H_2O_2 by treatment with SOD. Treatment with catalase substantially reduced the signal suggesting that fluorescence signal is mostly due to the production of H_2O_2. These results show that induction of CYP1B1 by Ahr agonists induced ROS both in the mitochondrial and microsomal fractions.

We also assessed the effects of *Cyp1b1* expression on mitochondrial electron transport complexes I (NADH-ubiquinone oxidoreductase, rotenone-sensitive) and IV (cytochrome *c* oxidase) activities. Complex I activity was inhibited by about 30% in lung mitochondria from both BaP- and TCDD-treated WT mice; however, there was no inhibition of these activities in *Cyp1b1*-null mice (Fig. 10*A*). CcO activity was inhibited by 30–40% by both BaP and TCDD in WT mice but not in *Cyp1b1*-null mice (Fig. 10*B*). By contrast, TCDD marginally induced CcO activity in the *Cyp1b1*-null mice; the reason for this increase is not presently clear. These results collectively demonstrate that CYP1B1 is targeted to mitochondria in the pulmonary tissue in response to PAH treatment and that CYP1B1 expression induces oxidative stress and partial loss of electron transport chain complex activities.

Damage to mtDNA is an important indicator of mitochondrial oxidative stress and also functional damage. Long stretches of (10 kb) mtDNA amplification from lung tissue showed that both BaP (Fig. 10, *C* and *E*) and TCDD (Fig. 10, *D* and *E*) induced mtDNA damage in WT mice but not in *Cyp1b1*-null mice. Notably, BaP induced about 50% mtDNA loss in *Cyp1a1/1a2*-null mice, which was marginally higher than in WT mice (40%). This is consistent with the high levels of CYP1B1 protein in *Cyp1a1/1a2*-null mice treated with BaP or TCDD. These results collectively show that Ahr-induced expression of CYP1B1 is a major contributing factor in mitochondrial dysfunction and mtDNA loss and that CYP1A1 plays minor role in this toxicity.

Relative Contributions of Microsomal and Mitochondrial CYP1B1 in Inducing Mitochondrial Dysfunction—To evaluate the relative contributions of the mitochondrial and microsomal CYP1B1 in mtDNA damage and mitochondrial dysfunction, we partially knocked down the microsomal NPR and mitochondrial Adx in human A549 cells because it is a lung-derived cell line and also because of the relatively low levels of NPR and Adx in these cells. Four different shRNAs cloned in pGFP-V-RS retroviral vector were procured from Origene and tested for their efficiency using transient transfections in A549 cells. Cell extracts were analyzed by immunoblotting 72 h after transfection (Fig. 11*A*). The most efficient shRNA constructs, NPR2 and Adx4, each producing about 60–70% reduction in protein levels, were used for generating stable A549 cell lines. The scrambled shRNA did not have any effect on the levels of NPR and Adx (Fig. 11*A*). The Adx and NPR protein levels, measured by immunoblot analysis, showed a suppression of ~60–70% in

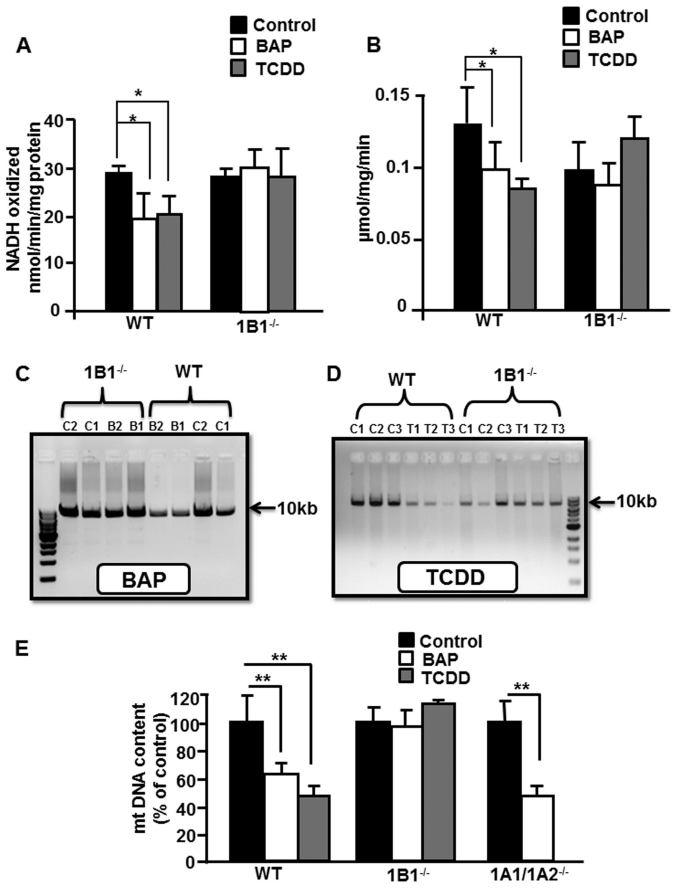

FIGURE 10. **Mitochondrial respiratory complex activities and mtDNA content in response to BaP and TCDD treatment in mouse lungs.** *A*, rotenone-sensitive complex I activity was measured in the lung mitochondria from control and *Cyp1b1*-null mice, treated with BaP or TCDD as NADH oxidation (decrease in absorbance at 340 nm). *B*, CcO activity was measured spectrophotometrically by following the oxidation of ferrocytochrome *c* at 550 nm. The details are described under the "Experimental Procedures." Data are presented as means ± S.D. from six different mice, and groups were compared using an unpaired, two-tailed Student's *t* test. *, $p < 0.05$. *C* and *D*, total DNA was isolated from lung slices from control, BaP-, and TCDD-treated WT, *Cyp1a1/1a2*-null, and *Cyp1b1*-null mice. Quantitative PCR was performed with 50 ng of the template DNA using van Houten's methodology as described under the "Experimental Procedures" and resolved on 0.6% (w/v) agarose gels. *E*, *bar graph* showing the relative mtDNA content in the treated and untreated groups from WT and *Cyp1b1*-null mouse lungs. Primers used are listed under the "Experimental Procedures." Data are presented as mean ± S.D. from six different mice, and groups were compared using an unpaired two-tailed Student's *t* test. *, $p < 0.05$; **, $p < 0.001$.

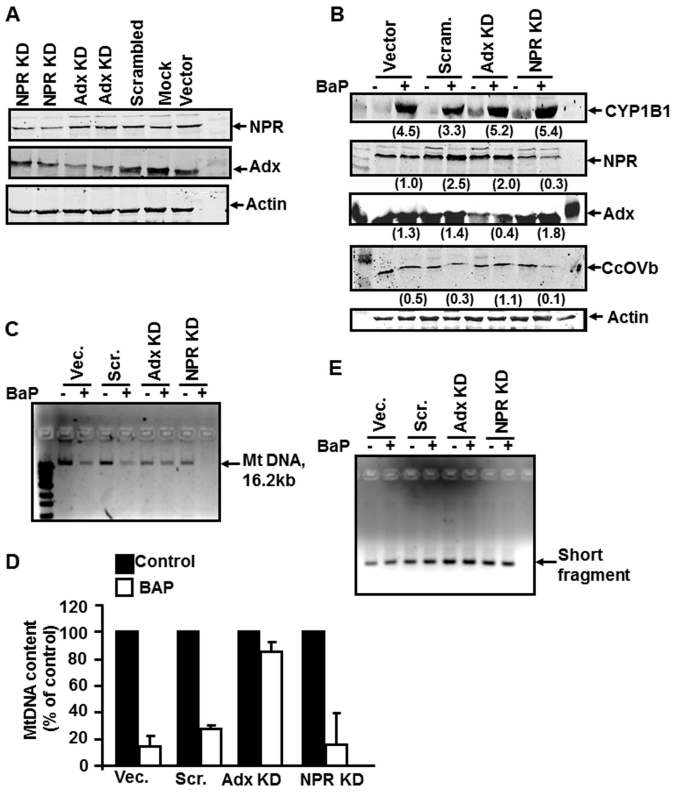

FIGURE 11. **Relative contributions of microsomal and mitochondrial CYP1B1 in inducing mitochondrial dysfunction.** *A*, shRNA constructs targeted for NPR and Adx mRNAs were transfected in A549 cells. The crude lysates were analyzed 48 h post-transfection by immunoblotting with NPR antibody (1:2500, v/v) and Adx antibody (1:1000, v/v). *B*, shRNA constructs showing the maximum knockdown in *A* were used to generate stable expression lines in A549 cells as described under the "Experimental Procedures." The cells were treated with DMSO alone or 20 μM BaP in DMSO for 72 h. Total cell lysate (50 μg of protein each) was subjected to immunoblot analysis with the indicated antibodies. The *numbers below* each lane represent relative band intensity for individual proteins. The values are average of two experiments. *C–E*, A549 cells stably expressing scrambled shRNA or shRNA for Adx and NPR were grown for 96 h either in presence of vehicle, DMSO alone, or with 20 μM BaP. mtDNA was quantified as in Fig. 10. *C*, ethidium bromide-stained pattern of 16.2-kb amplicon of mtDNA. *D*, PCR amplification of short mitochondrial fragment (100 bp) from different cell types treated with or without BaP as a template control. *E*, *bar graph* showing relative levels of mtDNA in different cell types treated with or without BaP. Details were as in Fig. 1 and under "Experimental Procedures."

the construct NPR2 and Adx4 (Fig. 11*A*). The BaP toxicity in stable A549 cells was tested by treating cells with 20 μM BaP for 72 h, and cells were treated similarly with DMSO as controls. CYP1B1 was induced in all cases, as revealed by the immunoblotting (Fig. 11*B*). NPR levels in NPR shRNA-expressing cells (NPR KD) showed a 50–60% reduction in both BaP-treated and untreated cells. Similarly, Adx levels were reduced by 60–70% in Adx shRNA-expressing cells (Adx KD). The effect of NPR and Adx knockdown on CcOVb levels, a key component of mitochondrial electron transport chain after 72 h of BaP treatment, was also studied. The level of CcOVb protein was decreased after BaP treatment in control cells. In cells expressing shRNA against Adx, there was significant protection, although similar protection against BaP-mediated decline was not observed in cells expressing shRNA against NPR mRNA.

The gel patterns of long stretch mtDNA amplification (Fig. 11*C*) and quantification (Fig 11*D*) show that mtDNA was markedly damaged in cells expressing control vector, scrambled vector, and shRNA for NPR (Fig. 11, *C* and *D*). However, mtDNA damage was only marginal in cells expressing shRNA for Adx (Fig 11*C*). The short stretch amplicon, used as template control, was also not affected in any of the cell lines or by BaP treatment (Fig. 11*E*). These results provide strong support for the role of mitochondrion-targeted CYP1B1 and its metabolic activity in inducing mtDNA damage and mitochondrial dysfunction.

DISCUSSION

The family 1 P450s play a critical role not only in the conversion of various PAHs to ultimate carcinogens but also in their clearance/excretion. CYP1A1, in particular, is thought to be important in efficient clearance of PAHs, and CYP1B1 is thought be important in inducing toxicity in different tissues (64, 65). The role of CYP1A2 in the metabolism of PAHs is

more limited, and it is thought to play a more important role in the metabolism of physiological substrates (66). In this study using MCF-7 breast carcinoma and A549 lung carcinoma cells, both of which express *Cyp1* genes in response to PAHs, and also lungs from WT, *Cyp1a1/1a2*-null, and *Cyp1b1*-null mice, we showed that human CYP1B1 is targeted to mitochondria through a pathway similar to that shown for rat and mouse CYP1A1 (32, 35, 37). We also show that mitochondrion-targeted CYP1B1 exhibits high AHH activity and most likely contributes to PAH-induced mitochondrial respiratory dysfunction and mtDNA loss.

We used four well established and widely used approaches, *viz.* protein import into isolated rat liver mitochondria and transient transfection in COS-7 cells for demonstrating mitochondrial targeting of human CYP1B1. First, mitochondrial localization of CYP1B1 in BaP-treated cells and lungs of treated mice was ascertained by limited trypsin digestion under conditions when the ER-associated protein is completely degraded, although the protein compartmentalized in the matrix compartment is resistant. Second, transient transfection in COS-7 cells (which do not express endogenous CYP1B1) showed that the N-terminal truncated (+34CYP1B1) protein colocalized with mitochondrion-specific CcOI at a higher level than the WT protein, as determined by immunofluorescence microscopy. Transfection of COS-7 cells with WT CYP1B1 cDNA along with cDNA encoding a catalytically active Ser protease, characterized before in our laboratory (AK131261), markedly increased co-localization of CYP1B1 with mitochondrial markers. Third, immunogold electron microscopy demonstrated a markedly higher number of electron-dense particles in trypsin-treated mitochondria from WT CYP1B1 cDNA-transfected cells as compared with mitochondria from mock-transfected cells. Finally, as shown for other constitutive and drug-inducible CYPs imported into mitochondria (35, 37–39, 48, 61), the mitochondrion-associated CYP1B1 was organized in a membrane-extrinsic manner as against membrane-intrinsic topology of ER-associated CYP1B1. These results demonstrate mitochondrial localization of CYP1B1 and its distinctive membrane association.

A direct way to demonstrate N-terminal processing of CYP1B1 protein imported into mitochondria is to purify the protein and determine its N-terminal sequence, similar to that carried out with purified CYP1A1 (37). In repeated attempts, however, we were unable to purify mitochondrial CYP1B1 in sufficient quantity either from BaP-induced MCF-7 cells or mouse lung mitochondria for N-terminal sequencing. It should be noted that CYP1B1 has not been purified from any mammalian sources thus far, possibly because of the low level of expression and the low mitochondrial yield from extrahepatic tissues. We therefore used several alternative approaches to demonstrate that N-terminal processed protein is imported into mitochondria and that the processing occurs in the cytoplasmic compartment of cells. 1) Transient transfection of COS-7 cells with WT CYP1B1 cDNA yielded only a small amount of mitochondrial CYP1B1, which was substantially increased by co-transfection with catalytically active polyserase cDNA (AK131261), and the increase was dependent on the dose of polyserase cDNA used. In a previous study, we showed that COS-7 cells contained polyserase activity, albeit at low levels (32). This basal level of polyserase activity is probably responsible for the low mitochondrial import of transiently expressed CYP1B1. 2) Mitochondrial CYP1B1 protein from cells transfected with WT CYP1B1 construct migrated marginally faster than the microsomal CYP1B1 on high resolution Tricine electrophoretic gels, suggesting that the former may be processed. The N-terminal processing was confirmed using N-terminally fused DHFR-CYP1B1 fusion protein. When co-expressed with polyserase cDNA, the ~90-kDa fusion protein was cleaved into an ~57-kDa protein, which cross-reacted with antibody to CYP1B1, and an ~33-kDa protein (29-kDa DHFR plus ~4-kDa 1B1), which did not cross-react with CYP1B1 antibody. Only the ~57-kDa CYP1B1 antibody-reactive fragment is localized in mitochondria and rendered resistant to trypsin action. These results confirm that the CYP1B1 N terminus contains a Ser protease cleavage site, and processing at this site by a cytosolic endoprotease is part of the mechanism for importing CYP1B1 to mitochondria. 3) Ala scanning mutations at the putative Ser protease processing site affected polyserase-mediated processing of the fusion protein as well as mitochondrial import of CYP1B1. Mutations at the 37/38 and 40/41 amino acid residues had a more pronounced effect on mitochondrial import. Sequence positions 37–41 also showed consensus for Ser protease processing. Notably, the processing site is just N-terminal to the putative mitochondrial import signal sequence at 43–48 and thus separated from the Ser protease site. Although results are not presented, mutations R38A and R41A of the +34/1B1 cDNA did not affect the mitochondrial import efficiency. Only substitutions at R41A, R43A, R44A, R45A, and R48A affected mitochondrial import efficiency. Although we have not been able to pinpoint the residue involved in processing, the sequence motif 37–41 most likely provides the recognition site for the polyserase processing.

We used a fluorometric method (52) for assaying BaP hydroxylation by mitochondrial and microsomal CYP1 proteins. This was based on previous studies by Guengerich and co-workers (26, 27) showing efficient metabolism of BaP by both CYP1A1 and CYP1B1 HPLC-based quantification of metabolites. Additionally, many soluble proteins, including Adx and to some extent Adr, are lost during rigorous purification steps, including digitonin treatment (35). Mitochondrial assay mixtures were therefore supplemented with optimal levels of Adx and AdxR. Although not shown, addition of NPR to the microsomal fraction of cells and tissues did not increase activity. Thus, the assays with both mitochondrial and microsomal enzymes and purified CYP1B1 were carried out under optimum electron transfer conditions. We showed that mitochondria from BaP- and TCDD-treated MCF-7 cells and mouse lung exhibit higher than the respective microsomal AHH activities. A higher AHH activity was also observed with purified CYP1B1 reconstituted with Adx + Adr than with NPR. Additionally, most of the mitochondrial AHH activity was inhibited by TMS, a CYP1B1-specific inhibitor. In line with previous studies showing very low AHH activity of mitochondrial CYP1A1 (59, 60), these results suggest that a large part of mitochondrial AHH activity is due to mitochondrial CYP1B1.

Real time PCR-based quantitation of *Cyp1* mRNAs from transgenic knock-out mice yielded unexpectedly high levels of

BaP- and TCDD-mediated induction of mRNAs. The *Cyp1b1* mRNA levels were induced nearly 400-fold in *Cyp1a1/1a2*-null mice, and similarly *Cyp1a1* and *-1a2* mRNAs were induced near 400-fold in *Cyp1b1*-null mice. Although intriguing, these results are consistent with previous studies from the Nebert laboratory showing near 1000-fold (0.003 to 82 mol of mRNA relative to β-actin mRNA induction of *Cyp1a1* mRNA in *Cyp1a2*-null mice and a similar extent of induction of *Cyp1a2* mRNA in *Cyp1a1*-null mice). The precise mechanism of intergenic regulation of *Cyp1* genes remains unclear.

Consistent with the high mitochondrial AHH activity in lungs of *Cyp1a1/1a2*-null mice as opposed to low activity in *Cyp1b1*-null mice, mitochondrial ROS production was nearly 2-fold higher in the former. Similarly, PAH-induced inhibition of mitochondrial complex I and complex IV activities were attenuated in *Cyp1b1*-null mice. Additionally, BaP- and TCDD-mediated mtDNA depletion was attenuated in *Cyp1b1*-null mice but not in *Cyp1a1/1a2*-null mice. A significant observation of this study is that both BaP- and TCDD-mediated effects on mitochondrial function were blunted in *Cyp1b1*-null mice. These results further confirm the role of CYP1B1 expression and its metabolic activity in mitochondrial dysfunction.

Results with A549 cells stably expressing shRNA against NPR and Adx mRNAs provided direct proof for the role of mitochondrial CYP1B1 in inducing mitochondrial dysfunction. Although the levels of NPR and Adx mRNA depletion in these cells reached only about 60–70%, the AHH activity of pre-digitonin mitochondria from Adx mRNA knockdown cells was 89 ± 5 pmol (product formed)/mg of protein/min as compared with 425–435 pmol (product formed)/mg of protein/min in similarly isolated mitochondria from cells expressing scrambled shRNA and NPR shRNA. Furthermore, the mtCYP contents were not affected by expressing shRNA to Adx or NPR. Results clearly show that PAH-induced degradation of CcOVb protein and depletion of mtDNA are attenuated in Adx shRNA-expressing cells but not in NPR shRNA-expressing cells. These results are consistent with the higher mitochondrial AHH activity and higher mitochondrial damage in cells and lungs that were induced to express CYP1B1.

In summary, these results show that mitochondrial targeting of CYP1B1 involves proteolytic processing of the N terminus of the nascent protein by a cytosolic endoprotease. In this respect, the endoprotease processing mechanism appears to be conserved among family 1 CYPs. Protein sequence analysis also suggests the presence of Ser protease cleavage site at the N terminus of CYP1A2. Further experiments are needed to ascertain if the Ser protease processing mechanism also applies to the mitochondrial import of CYP1A2. Our results also suggest that, in contrast to the mitochondrial CYP1A1, mitochondrial CYP1B1 exhibits remarkably high AHH activity, which is most likely involved in inducing PAH-mediated mitochondrial dysfunction.

Acknowledgments—We are thankful to members of the Avadhani laboratory for their useful comments and suggestions and to Dr. Daniel Nebert for providing Cyp1a1/1a2-null mice.

REFERENCES

1. McKay, J. A., Murray, G. I., Ah-See, A. K., Greenlee, W. F., Marcus, C. B., Burke, M. D., and Melvin, W. T. (1996) Differential expression of CYP1A1 and CYP1B1 in human breast cancer. *Biochem. Soc. Trans.* **24,** 327S
2. Conney, A. H. (1982) Induction of microsomal enzymes by foreign chemicals and carcinogenesis by polycyclic aromatic hydrocarbons: G. H. A. Clowes Memorial Lecture. *Cancer Res.* **42,** 4875–4917
3. Kim, D., and Guengerich, F. P. (2005) Cytochrome P450 activation of arylamines and heterocyclic amines. *Annu. Rev. Pharmacol. Toxicol.* **45,** 27–49
4. Gelboin, H. V. (1980) Benzo[α]pyrene metabolism, activation and carcinogenesis: role and regulation of mixed-function oxidases and related enzymes. *Physiol. Rev.* **60,** 1107–1166
5. Jerina, D. M. (1983) The 1982 Bernard B. Brodie Award Lecture. Metabolism of aromatic hydrocarbons by the cytochrome P-450 system and epoxide hydrolase. *Drug Metab. Dispos.* **11,** 1–4
6. Miller, K. P., and Ramos, K. S. (2001) Impact of cellular metabolism on the biological effects of benzo[a]pyrene and related hydrocarbons. *Drug Metab. Rev.* **33,** 1–35
7. Gonzalez, F. J., Jaiswal, A. K., and Nebert, D. W. (1986) P450 genes: evolution, regulation, and relationship to human cancer and pharmacogenetics. *Cold Spring Harbor Symp. Quant. Biol.* **51,** 879–890
8. Nebert, D. W., Jaiswal, A. K., Meyer, U. A., and Gonzalez, F. J. (1987) Human P-450 genes: evolution, regulation and possible role in carcinogenesis. *Biochem. Soc. Trans.* **15,** 586–589
9. Nebert, D. W., Dalton, T. P., Okey, A. B., and Gonzalez, F. J. (2004) Role of aryl hydrocarbon receptor-mediated induction of the CYP1 enzymes in environmental toxicity and cancer. *J. Biol. Chem.* **279,** 23847–23850
10. Schweikl, H., Taylor, J. A., Kitareewan, S., Linko, P., Nagorney, D., and Goldstein, J. A. (1993) Expression of CYP1A1 and CYP1A2 genes in human liver. *Pharmacogenetics* **3,** 239–249
11. Hankinson, O. (1995) The aryl hydrocarbon receptor complex. *Annu. Rev. Pharmacol. Toxicol.* **35,** 307–340
12. Nebert, D. W., Roe, A. L., Dieter, M. Z., Solis, W. A., Yang, Y., and Dalton, T. P. (2000) Role of the aromatic hydrocarbon receptor and [Ah] gene battery in the oxidative stress response, cell cycle control, and apoptosis. *Biochem. Pharmacol.* **59,** 65–85
13. Shimada, T., Hayes, C. L., Yamazaki, H., Amin, S., Hecht, S. S., Guengerich, F. P., and Sutter, T. R. (1996) Activation of chemically diverse procarcinogens by human cytochrome P-450 1B1. *Cancer Res.* **56,** 2979–2984
14. Sutter, T. R., Tang, Y. M., Hayes, C. L., Wo, Y. Y., Jabs, E. W., Li, X., Yin, H., Cody, C. W., and Greenlee, W. F. (1994) Complete cDNA sequence of a human dioxin-inducible mRNA identifies a new gene subfamily of cytochrome P450 that maps to chromosome 2. *J. Biol. Chem.* **269,** 13092–13099
15. Hakkola, J., Pasanen, M., Pelkonen, O., Hukkanen, J., Evisalmi, S., Anttila, S., Rane, A., Mäntylä, M., Purkunen, R., Saarikoski, S., Tooming, M., and Raunio, H. (1997) Expression of CYP1B1 in human adult and fetal tissues and differential inducibility of CYP1B1 and CYP1A1 by Ah receptor ligands in human placenta and cultured cells. *Carcinogenesis* **18,** 391–397
16. Tang, Y. M., Chen, G. F., Thompson, P. A., Lin, D. X., Lang, N. P., and Kadlubar, F. F. (1999) Development of an antipeptide antibody that binds to the C-terminal region of human CYP1B1. *Drug Metab. Dispos.* **27,** 274–280
17. Edwards, R. J., Adams, D. A., Watts, P. S., Davies, D. S., and Boobis, A. R. (1998) Development of a comprehensive panel of antibodies against the major xenobiotic metabolising forms of cytochrome P450 in humans. *Biochem. Pharmacol.* **56,** 377–387
18. Dutheil, F., Beaune, P., and Loriot, M. A. (2008) Xenobiotic metabolizing enzymes in the central nervous system: Contribution of cytochrome P450 enzymes in normal and pathological human brain. *Biochimie* **90,** 426–436
19. Murray, G. I., Taylor, V. E., McKay, J. A., Weaver, R. J., Ewen, S. W., Melvin, W. T., and Burke, M. D. (1995) The immunohistochemical localization of drug-metabolizing enzymes in prostate cancer. *J. Pathol.* **177,** 147–152
20. Murray, G. I., Taylor, M. C., McFadyen, M. C., McKay, J. A., Greenlee,

W. F., Burke, M. D., and Melvin, W. T. (1997) Tumor-specific expression of cytochrome P450 CYP1B1. *Cancer Res.* **57,** 3026–3031
21. Buters, J. T., Sakai, S., Richter, T., Pineau, T., Alexander, D. L., Savas, U., Doehmer, J., Ward, J. M., Jefcoate, C. R., and Gonzalez, F. J. (1999) Cytochrome P450 CYP1B1 determines susceptibility to 7,12-dimethylbenz[*a*]anthracene-induced lymphomas. *Proc. Natl. Acad. Sci. U.S.A.* **96,** 1977–1982
22. Hayes, C. L., Spink, D. C., Spink, B. C., Cao, J. Q., Walker, N. J., and Sutter, T. R. (1996) 17β-Estradiol hydroxylation catalyzed by human cytochrome P450 1B1. *Proc. Natl. Acad. Sci. U.S.A.* **93,** 9776–9781
23. McKay, J. A., Melvin, W. T., Ah-See, A. K., Ewen, S. W., Greenlee, W. F., Marcus, C. B., Burke, M. D., and Murray, G. I. (1995) Expression of cytochrome P450 CYP1B1 in breast cancer. *FEBS Lett.* **374,** 270–272
24. Badawi, A. F., Cavalieri, E. L., and Rogan, E. G. (2001) Role of human cytochrome P450 1A1, 1A2, 1B1, and 3A4 in the 2-, 4-, and 16-α-hydroxylation of 17β-estradiol. *Metabolism* **50,** 1001–1003
25. Lee, A. J., Cai, M. X., Thomas, P. E., Conney, A. H., and Zhu, B. T. (2003) Characterization of the oxidative metabolites of 17β-estradiol and estrone formed by 15 selectively expressed human cytochrome p450 isoforms. *Endocrinology* **144,** 3382–3398
26. Shimada, T., Watanabe, J., Inoue, K., Guengerich, F. P., and Gillam, E. M. (2001) Specificity of 17β-oestradiol and benzo[a]pyrene oxidation by polymorphic human cytochrome P4501B1 variants substituted at residues 48, 119 and 432. *Xenobiotica* **31,** 163–176
27. Shimada, T., Watanabe, J., Kawajiri, K., Sutter, T. R., Guengerich, F. P., Gillam, E. M., and Inoue, K. (1999) Catalytic properties of polymorphic human cytochrome P450 1B1 variants. *Carcinogenesis* **20,** 1607–1613
28. Tsuchiya, Y., Nakajima, M., Kyo, S., Kanaya, T., Inoue, M., and Yokoi, T. (2004) Human CYP1B1 is regulated by estradiol via estrogen receptor. *Cancer Res.* **64,** 3119–3125
29. Vasiliou, V., and Gonzalez, F. J. (2008) Role of CYP1B1 in glaucoma. *Annu. Rev. Pharmacol. Toxicol.* **48,** 333–358
30. Bagiyeva, S., Marfany, G., Gonzalez-Angulo, O., and Gonzalez-Duarte, R. (2007) Mutational screening of CYP1B1 in Turkish PCG families and functional analyses of newly detected mutations. *Mol. Vis.* **13,** 1458–1468
31. Sangar, M. C., Bansal, S., and Avadhani, N. G. (2010) Bimodal targeting of microsomal cytochrome P450s to mitochondria: implications in drug metabolism and toxicity. *Expert Opin. Drug Metab. Toxicol.* **6,** 1231–1251
32. Boopathi, E., Srinivasan, S., Fang, J. K., and Avadhani, N. G. (2008) Bimodal protein targeting through activation of cryptic mitochondrial targeting signals by an inducible cytosolic endoprotease. *Mol. Cell* **32,** 32–42
33. Anandatheerthavarada, H. K., Sepuri, N. B., and Avadhani, N. G. (2009) Mitochondrial targeting of cytochrome P450 proteins containing NH_2-terminal chimeric signals involves an unusual TOM20/TOM22 bypass mechanism. *J. Biol. Chem.* **284,** 17352–17363
34. Sepuri, N. B., Yadav, S., Anandatheerthavarada, H. K., and Avadhani, N. G. (2007) Mitochondrial targeting of intact CYP2B1 and CYP2E1 and N-terminal truncated CYP1A1 proteins in *Saccharomyces cerevisiae*–role of protein kinase A in the mitochondrial targeting of CYP2E1. *FEBS J.* **274,** 4615–4630
35. Dasari, V. R., Anandatheerthavarada, H. K., Robin, M. A., Boopathi, E., Biswas, G., Fang, J. K., Nebert, D. W., and Avadhani, N. G. (2006) Role of protein kinase C-mediated protein phosphorylation in mitochondrial translocation of mouse CYP1A1, which contains a non-canonical targeting signal. *J. Biol. Chem.* **281,** 30834–30847
36. Bhagwat, S. V., Biswas, G., Anandatheerthavarada, H. K., Addya, S., Pandak, W., and Avadhani, N. G. (1999) Dual targeting property of the N-terminal signal sequence of P4501A1. Targeting of heterologous proteins to endoplasmic reticulum and mitochondria. *J. Biol. Chem.* **274,** 24014–24022
37. Addya, S., Anandatheerthavarada, H. K., Biswas, G., Bhagwat, S. V., Mullick, J., and Avadhani, N. G. (1997) Targeting of NH_2-terminal-processed microsomal protein to mitochondria: a novel pathway for the biogenesis of hepatic mitochondrial P450MT2. *J. Cell Biol.* **139,** 589–599
38. Anandatheerthavarada, H. K., Addya, S., Dwivedi, R. S., Biswas, G., Mullick, J., and Avadhani, N. G. (1997) Localization of multiple forms of inducible cytochromes P450 in rat liver mitochondria: immunological characteristics and patterns of xenobiotic substrate metabolism. *Arch. Biochem. Biophys.* **339,** 136–150
39. Anandatheerthavarada, H. K., Biswas, G., Mullick, J., Sepuri, N. B., Otvos, L., Pain, D., and Avadhani, N. G. (1999) Dual targeting of cytochrome P4502B1 to endoplasmic reticulum and mitochondria involves a novel signal activation by cyclic AMP-dependent phosphorylation at ser128. *EMBO J.* **18,** 5494–5504
40. Robin, M. A., Anandatheerthavarada, H. K., Biswas, G., Sepuri, N. B., Gordon, D. M., Pain, D., and Avadhani, N. G. (2002) Bimodal targeting of microsomal CYP2E1 to mitochondria through activation of an N-terminal chimeric signal by cAMP-mediated phosphorylation. *J. Biol. Chem.* **277,** 40583–40593
41. Sangar, M. C., Anandatheerthavarada, H. K., Tang, W., Prabu, S. K., Martin, M. V., Dostalek, M., Guengerich, F. P., and Avadhani, N. G. (2009) Human liver mitochondrial cytochrome P450 2D6–individual variations and implications in drug metabolism. *FEBS J.* **276,** 3440–3453
42. Sangar, M. C., Anandatheerthavarada, H. K., Martin, M. V., Guengerich, F. P., and Avadhani, N. G. (2010) Identification of genetic variants of human cytochrome P450 2D6 with impaired mitochondrial targeting. *Mol. Genet. Metab.* **99,** 90–97
43. Robin, M. A., Prabu, S. K., Raza, H., Anandatheerthavarada, H. K., and Avadhani, N. G. (2003) Phosphorylation enhances mitochondrial targeting of GSTA4–4 through increased affinity for binding to cytoplasmic Hsp70. *J. Biol. Chem.* **278,** 18960–18970
44. Boopathi, E., Anandatheerthavarada, H. K., Bhagwat, S. V., Biswas, G., Fang, J. K., and Avadhani, N. G. (2000) Accumulation of mitochondrial P450MT2, NH_2-terminal truncated cytochrome P4501A1 in rat brain during chronic treatment with β-naphthoflavone. A role in the metabolism of neuroactive drugs. *J. Biol. Chem.* **275,** 34415–34423
45. Robin, M. A., Anandatheerthavarada, H. K., Fang, J. K., Cudic, M., Otvos, L., and Avadhani, N. G. (2001) Mitochondrial targeted cytochrome P450 2E1 (P450 MT5) contains an intact N terminus and requires mitochondrial specific electron transfer proteins for activity. *J. Biol. Chem.* **276,** 24680–24689
46. Shi, Z., Dragin, N., Miller, M. L., Stringer, K. F., Johansson, E., Chen, J., Uno, S., Gonzalez, F. J., Rubio, C. A., and Nebert, D. W. (2010) Oral benzo[*a*]pyrene-induced cancer: two distinct types in different target organs depend on the mouse Cyp1 genotype. *Int. J. Cancer* **127,** 2334–2350
47. Bhagwat, S. V., Mullick, J., Raza, H., and Avadhani, N. G. (1999) Constitutive and inducible cytochromes P450 in rat lung mitochondria: xenobiotic induction, relative abundance, and catalytic properties. *Toxicol. Appl. Pharmacol.* **156,** 231–240
48. Anandatheerthavarada, H. K., Vijayasarathy, C., Bhagwat, S. V., Biswas, G., Mullick, J., and Avadhani, N. G. (1999) Physiological role of the N-terminal processed P4501A1 targeted to mitochondria in erythromycin metabolism and reversal of erythromycin-mediated inhibition of mitochondrial protein synthesis. *J. Biol. Chem.* **274,** 6617–6625
49. Laemmli, U. K. (1970) Cleavage of structural proteins during the assembly of the head of bacteriophage T4. *Nature* **227,** 680–685
50. Wu, M., Neilson, A., Swift, A. L., Moran, R., Tamagnine, J., Parslow, D., Armistead, S., Lemire, K., Orrell, J., Teich, J., Chomicz, S., and Ferrick, D. A. (2007) Multiparameter metabolic analysis reveals a close link between attenuated mitochondrial bioenergetic function and enhanced glycolysis dependency in human tumor cells. *Am. J. Physiol. Cell Physiol.* **292,** C125–C136
51. Clark, B. J., and Waterman, M. R. (1991) The hydrophobic amino-terminal sequence of bovine 17α-hydroxylase is required for the expression of a functional hemoprotein in COS 1 cells. *J. Biol. Chem.* **266,** 5898–5904
52. Nebert, D. W., and Gelboin, H. V. (1968) Substrate-inducible microsomal aryl hydroxylase in mammalian cell culture. I. Assay and properties of induced enzyme. *J. Biol. Chem.* **243,** 6242–6249
53. Omura, T., and Sato, R. (1964) The carbon monoxide-binding pigment of liver microsomes. II. solubilization, purification, and properties. *J. Biol. Chem.* **239,** 2379–2385
54. Guengerich, F. P., Dannan, G. A., Wright, S. T., Martin, M. V., and Kaminsky, L. S. (1982) Purification and characterization of liver microsomal cytochromes p-450: electrophoretic, spectral, catalytic, and immunochemical properties and inducibility of eight isozymes isolated from rats treated with Phenobarbital or β-naphthoflavone. *Biochemistry* **21,**

6019–6030
55. Prabu, S. K., Anandatheerthavarada, H. K., Raza, H., Srinivasan, S., Spear, J. F., and Avadhani, N. G. (2006) Protein kinase A-mediated phosphorylation modulates cytochrome *c* oxidase function and augments hypoxia and myocardial ischemia-related injury. *J. Biol. Chem.* **281,** 2061–2070
56. Birch-Machine, M. A., and Turnbull, D. M. (2001) Assaying mitochondrial respiratory complex activity in mitochondria isolated from human cells and tissues. *Methods Cell Biol.* **65,** 97–117
57. Bansal, S., Liu, C. P., Sepuri, N. B., Anandatheerthavarada, H. K., Several, V., Hook, J., Milne, G. L., Guengerich, F. P., and Avadhani, N. G. (2010) Mitochondria-targeted cytochrome P450 2E1 induces oxidative damage and augments alcohol-mediated oxidative stress. *J. Biol. Chem.* **285,** 24609–24619
58. Yaks, F. M., and Van Houston, B. (1997) Mitochondrial DNA damage is more extensive and persists longer than nuclear DNA damage in human cells following oxidative stress. *Proc. Natl. Acad. Sci. U.S.A.* **94,** 514–519
59. Dong, H., Dalton, T. P., Miller, M. L., Chen, Y., Uno, S., Shi, Z., Shorter, H. G., Bansal, S., Avadhani, N. G., and Nebert, D. W. (2009) Knock-in mouse lines expressing either mitochondrial or microsomal CYP1A1: differing responses to dietary benzo[*a*]pyrene as proof of principle. *Mol. Pharmacol.* **75,** 555–567
60. Raza, H., and Avadhani, N. G. (1988) Hepatic mitochondrial cytochrome P-450 system. Purification and characterization of two distinct forms of mitochondrial cytochrome P-450 from β-naphthoflavone-induced rat liver. *J. Biol. Chem.* **263,** 9533–9541
61. Avadhani, N. G., Sangar, M. C., Bansal, S., and Baja, P. (2011) Bimodal targeting of cytochrome P450s to endoplasmic reticulum and mitochondria: the concept of chimeric signals. *FEBS J.* **278,** 4218–4229
62. Dragin, N., Uno, S., Wang, B., Dalton, T. P., and Nebert, D. W. (2007) Generation of 'humanized' hCYP1A1_1A2_Cyp1a1/1a2(−/−) mouse line. *Biochem. Biophys. Res. Commun.* **359,** 635–642
63. Liang, H. C., Li, H., McKinnon, R. A., Duffy, J. J., Potter, S. S., Pug, A., and Nebert, D. W. (1996) Cyp1a2(−/−) null mutant mice develop normally but show deficient drug metabolism. *Proc. Natl. Acad. Sci. U.S.A.* **93,** 1671–1676
64. Nebert, D. W., Shi, Z., Gales-Peralta, M., Uno, S., and Dragin, N. (2013) Oral benzo[*a*]pyrene: understanding pharmacokinetics, defoliation, and consequences–Cyp1 knockout mouse lines as a paradigm. *Mol. Pharmacol.* **84,** 304–313
65. Uno, S., Dalton, T. P., Dragin, N., Curran, C. P., Darkener, S., Miller, M. L., Shorter, H. G., Gonzalez, F. J., and Nebert, D. W. (2006) Oral benzo[*a*]pyrene in Cyp1 knockout mouse lines: CYP1A1 important in defoliation, CYP1B1 metabolism required for immune damage independent of total-body burden and clearance rate. *Mol. Pharmacol.* **69,** 1103–1114
66. Bauer, E., Guo, Z., Jeng, Y. F., Bell, L. C., Seldin, D., and Guengerich, F. P. (1995) Oxidation of benzo[*a*]pyrene by recombinant human cytochrome P450 enzymes. *Chem. Res. Toxicol.* **8,** 136–142